AD-A047 466 CARNEGIE-MELLON UNIV PITTSBURGH PA DEPT OF MECHANICA--ETC F/G 11/6
TWO CASES OF INCLUSION-INCLUSION INTERACTION IN A TI ALLOY.(U)
OCT 77 J L SWEDLOW, G B SINCLAIR AFOSR-76-2993

UNCLASSIFIED SM-77-7 AFOSR-TR-77-1290 NL

OF
AD
A047466

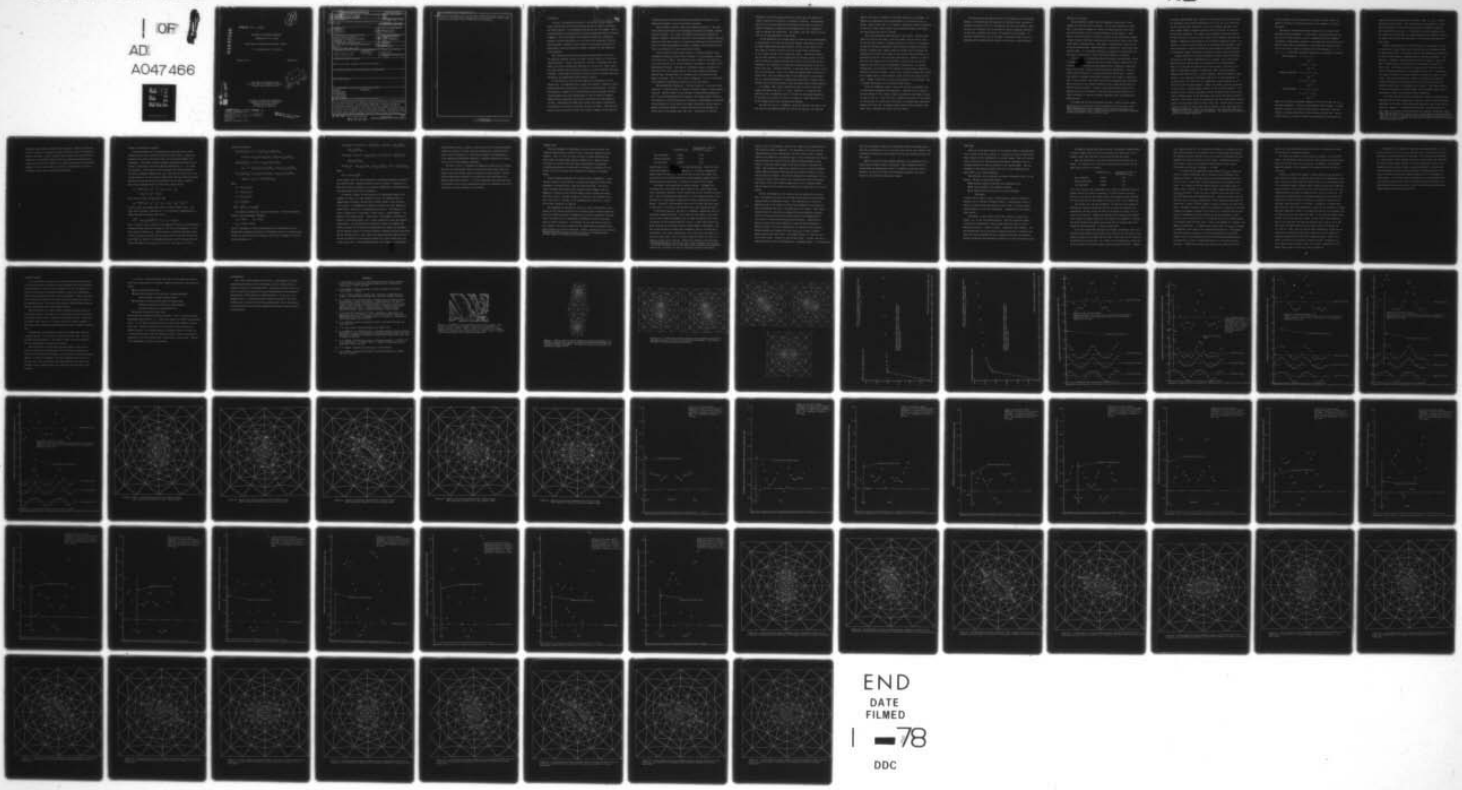

END
DATE FILMED
1 -78
DDC

AFOSR-TR- 77 - 1290

TWO CASES OF INCLUSION-INCLUSION INTERACTION IN A Ti ALLOY

(Final Report on Research Grant AFOSR 76-2993)

J. L. Swedlow and G. B. Sinclair

Report SM 77-7

October 1977

This work was supported by the
Air Force Office of Scientific Research
Research Grant AFOSR 76-2993

Department of Mechanical Engineering
Carnegie Institute of Technology
Carnegie Mellon University
Pittsburgh, Pennsylvania

SECURITY CLASSIFICATION OF THIS PAGE (When Data Entered)

REPORT DOCUMENTATION PAGE

READ INSTRUCTIONS BEFORE COMPLETING FORM

1. REPORT NUMBER: AFOSR-TR-77-1290	2. GOVT ACCESSION NO.
3. RECIPIENT'S CATALOG NUMBER	
4. TITLE (and Subtitle): TWO CASES OF INCLUSION-INCLUSION INTERACTION IN A Ti ALLOY.	5. TYPE OF REPORT & PERIOD COVERED: FINAL rept. 1 Apr 76-31 Aug 77
6. PERFORMING ORG. REPORT NUMBER	
7. AUTHOR(s): J. L. SWEDLOW, G. B. SINCLAIR	8. CONTRACT OR GRANT NUMBER(s): AFOSR-76-2993
9. PERFORMING ORGANIZATION NAME AND ADDRESS: CARNEGIE MELLON UNIVERSITY, DEPARTMENT OF MECHANICAL ENGINEERING, PITTSBURGH, PA 15213	10. PROGRAM ELEMENT, PROJECT, TASK AREA & WORK UNIT NUMBERS: 2307B2, 61102F
11. CONTROLLING OFFICE NAME AND ADDRESS: AIR FORCE OFFICE OF SCIENTIFIC RESEARCH/NA, BLDG 410, BOLLING AIR FORCE BASE, 20332	12. REPORT DATE: Oct 77
	13. NUMBER OF PAGES: 74
14. MONITORING AGENCY NAME & ADDRESS (if different from Controlling Office): SM-77-7	15. SECURITY CLASS. (of this report): UNCLASSIFIED
12 76p.	15a. DECLASSIFICATION/DOWNGRADING SCHEDULE

16. DISTRIBUTION STATEMENT (of this Report)

Approved for public release; distribution unlimited.

17. DISTRIBUTION STATEMENT (of the abstract entered in Block 20, if different from Report)

18. SUPPLEMENTARY NOTES

19. KEY WORDS (Continue on reverse side if necessary and identify by block number)

FRACTURE
MICROSTRUCTURE
MACROSTRUCTURE
FAILURE PROCESS
FINITE ELEMENT
PLASTICITY

20. ABSTRACT (Continue on reverse side if necessary and identify by block number)

A basic investigation was conducted to study the behavior of a continuous media with interacting inclusions. Material property data used for this study modeled an Alpha/Beta titanium. Finite Element simulation of the media included a generalized von-Mises yield criteria for plasticity. Uniaxial loading was considered with the parametric variations of the angle between the line of the inclusions and the load direction. Further three boundary displacement restrain conditions were considered. From these analyses the strain localization of the inclusion interaction was examined. The Final Report contains the analyses

DD FORM 1 JAN 73 1473 EDITION OF 1 NOV 65 IS OBSOLETE

UNCLASSIFIED

SECURITY CLASSIFICATION OF THIS PAGE (When Data Entered)

405 494

output data and computer plots of the region experiencing plastic strain. This research is continuing under a separate grant to investigate the strain localization at the inclusions and the formation of microcracks.

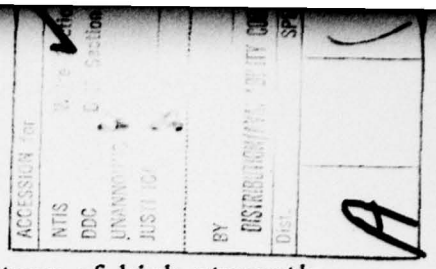

Introduction

An issue of considerable interest in the fracture of high strength alloys concerns the role of microstructure and how its behavior influences the failure process. As delineated by Cox and Low [1], for example, control of microstructure in selected steels can have a pronounced effect on fracture toughness. One of the features of the process whereby this influence is exerted is strain localization, as it has come to be designated, reference here being made to behavior in the vicinity of and between inclusions and particulates, which are otherwise intended to enhance the bulk properties of the material.

This issue has attracted the attention of metallurgists in the past few years; and Thompson, for one, has made a careful review [2] of this and allied literature. Several contributions, too many to enumerate here, were made at the recent International Conference on Fracture [3]. Other conferences and symposia within the metals community itself are similarly dedicated. In effect, a great deal of attention has been devoted to creating, observing, describing, and characterizing the processes involved.

At the same time, this issue has captured the imagination of a few mechanicists. In simplified terms, strain localization is related to stress concentration which historically is the object of such analysis. Of course the relation is complex in that stress analysis tends to presume straightforward geometric and load configurations as well as material response, whereas strain localization occurs under circumstances far more difficult to model. Nonetheless the effort goes forward, and careful contributions by such people as Drucker [4] and Rice [5] are to be found. These and other works are most provocative in that they carefully examine the metallurgical

literature and seek to draw therefrom issues deemed both essential to the problem and workable in terms of available techniques.

Such literature, however, tends to be slightly pessimistic. The mechanics problems associated with metallurgical observation are subtle, complex, and hard to define. In a sense, the problem almost becomes defining the problem. Moreover, the behavior involved in the processes leading to material failure are ones which remain to be resolved satisfactorily on the macroscale, where the continuum assumptions seem most reasonable, and transferring attention to a microscale is in some respects most trying.

We have chosen to address these issues in a slightly different manner. (Although discussing this point tends to become a bit philosophical, perhaps a few words are in order.) The information most evident to the mechanicist is his own capacity to set and solve problems, and broadly, the nature of the metallurgical findings. With respect to problem-solving, one develops the same sense that, given enough time on a big enough computer and adequate material data, the mechanicist can eventually solve any problem to some degree of accuracy. This is not so much a braggadocio as it is a reflection of the growth of computational mechanics over the last decade.

The metallurgical findings are - for the mechanicist - less easily characterized. If the discussion is limited to fracture, however, certain matters stand out. Material rupture in the presence of considerable yielding have yet to be well characterized by the engineer, even though efforts utilizing such measures as J and COD continue to be pressed. Metallographic examination of such failures is in any event still highly qualitative, and the tools regarded increasingly effective are those associated with fractography and certain types of microscopy (SEM, TEM, e.g.). Conclusions are perforce

inferential, but their growing reliability depends upon the emergence of certain similarities of behavior, or patterns of behavior. These developments have led to semi-quantitative techniques (which often draw upon correlative information as opposed to basic physics) and even a language of sorts to describe the observations. For example, the term "strain localization" is one whose popularity is but recent.

To the mechanicist the striking feature of these and allied developments is the physical size scale over which they operate. Observations are made of events ranging from sub-micron behavior to sizes on the order of $10^3\mu$. This range is dictated of course by use of various forms of microscopy; it is in sharp contrast to more traditional scales. Dislocation mechanics was for years regarded as the starting point for ultimate solution of fracture (or failure or rupture) problems and, while it still provides critical information, has apparently not succeeded in achieving answers at the multimicron size scale. Continuum mechanics, on the other hand, has proven successful on the macroscale - there is an immense literature hardly in need of discussion here - but the resolving power of such techniques is also limited. That is, continuum mechanics on a macroscale breaks down or contains demonstrable error on the scale typical of the microscopy used in failure analysis.

In a phrase, then, neither (theoretical) end of the size scale quite reaches the middle range (ca. 1μ - 100μ). Moreover, it is apparent that behavior at this intermediate scale is one which in some manner jumps from its lower end to its upper, and then to a larger one; there appears here to be the linkage between micro and macroscale behavior.

How does this occur? In mechanics, where the reflexive attitude is that size scale of any problem governs the scale of the response, this apparent

jump in size scale is certainly an intriguing question to investigate. In addition the significance of the problem makes it an important issue to pursue. What we need, then, is to contrive a problem or sequence of problems in which this jump is both unlikely and inevitable and them to seek means for articulating the event(s) involved.

How we have proceeded forms the basis of this report. Certain points should be noted at this stage, so that the context for the work is clear. We view the metallographic information depicted in Figure 1 as typifying a certain microstructure comprising a matrix having well defined inclusions. We know in advance that a modest degree of external load will produce concentrations of stress in the region of each inclusion-matrix interface; by association there will also be strain concentrations. Moreover, we anticipate that this behavior will be *localized* to each inclusion in that the range over which this occurs is demonstrably limited [6,7]. As external loading grows, we would hope to see evidence of local behavior linking up, from one inclusion to another, so that a zone of yield or plastic flow occurs over a pathway which is both extensive in one direction and limited in the other. Damage is expected to accrue in this pathway, by various means, and it becomes the precursor to the failure surface itself.

Given this framework, there is need to do the work at reasonable cost in terms both of peoplepower and computation. While the field in Figure 1 could be modeled *in toto*, doing so would be prohibitive and somewhat limited in what it tells us. Since the issue is interaction, however, we have chosen to consider only two inclusions at the outset, to identify their individual behavior with some care, to document their response under controlled conditions, and to interpret the results with due caution.

We have done this and report here what are considered to be our central findings. The modeling and the mechanics are discussed first, and then we describe the results of two sets of analyses, for each of two models. While obviously our "solutions" are in the form of extensive numerical printouts, we seek here to emphasize the nature and character of our findings. An extensive numerical data base is of course in hand, and we plan to use it in designing and interpreting other analyses as this work is carried forward.

MODELING OF INCLUSIONS

The overwhelming evidence from metallographic observations is that neighboring inclusions tend to interact. By the term, inclusion, we refer here to any material embedded in a matrix of another material, the elastic and plastic behavior of the two being different in some respects. Interaction, on the other hand, is less well defined* in that observations suggest a range of events from strain localization in some visible form, to void initiation, growth, and coalescence. The type(s) of interaction we would be able to discern would perforce depend upon what is admitted by a particular computational model. It was decided, therefore, to proceed on a step-by-step and necessarily cautious basis, taking conservative models at the outset.

Since the issue is interaction between inclusions, the model must include a minimum [illegible]. In order to reflect the actual physical situation the two inclusi[illegible]uld be spaced several diameters apart; adopting a conservative line, we have taken a center-to-center spacing of $11\frac{1}{2}$ diameters. This precludes elastic interaction, to judge from related studies [6,7]. Further, they should be arranged so that their orientation with respect to load direction is easily varied. This notion stems from the inference that interaction may be sensitive to the relative direction of the loading and the axis connecting the two inclusions. Finally, we are aware that the detail of any computed result may be sensitive to the particular element map used; an internal consistency is required to permit comparable bases for interpreting numerical data.

An element map was then constructed such that a central circular region containing the two inclusions could be rotated to several positions within

*Trial definitions are being formulated and are being tested against data of the sort presented here. A report on this portion of the work is deferred pending development of further baseline data.

an overall square element map. Relative to the vertical, the axis connecting the inclusions could assume the directions of 0, 22.5, 45, 67.5, and 90 deg. At the inclusion-matrix interface, a total of 24 elements was used to provide a modest degree of angular resolution, both for strains (or stresses) and for their gradients. The element size is graduated toward the interior of the inclusions, as well as to the exterior, first gradually and then more rapidly.* Mapping was facilitated by use of bipolar coordinates locally - see Figure 2. As may be seen in Figures 3a-3e, the intent outlined above to capture indications of inclusion interaction was provided for without creating an excessively complex element map that would be costly in initial analyses.

Loading conditions are another important but subtle aspect of modeling, and there are two primary characteristics to consider. One is the overall pattern involved, and the other is the specifics of its representation. While it is true that we need not at this stage assign a size scale to the model, we nonetheless regard it as physically small, with the inclusion spacing on the order of 100μm. Unless, therefore, the area of material under analysis is in a position of extremely high stress or strain gradients, as in the vicinity of a crack tip, it is sufficient to limit attention to uniform fields such as simple tension. Indeed, the results we report correspond to such a state. Lateral loading, however, is not so easily resolved. It is possible to have a lateral constraint such that no motion normal to the direction of loading occurs; on the other hand, there may be no lateral constraint whatever. Third, there may be an intermediate case which could involve lateral motion associated with a Poisson field of some sort. We felt that it would be useful to consider all three cases, for two reasons. First, there appeared to

*Mapping was checked by certain elastic analyses. The inclusions were represented as holes, and a patch test was performed. The results were satisfactory and will be reported separately.

be no clear basis for selecting one over the other two and, second, we deemed it advisable to develop some sense of the importance of lateral constraint.

The specific representation of the excitation was in terms of displacements along the boundary. In this manner, one could infer that some basic call is under analysis, and it is compatible with like neighbors. In addition, computational experience would suggest that the analysis would be more stable were we subsequently to extend excitation to high strains. Thus if the overall domain is characterized by the dimensions $-a < x < a$, $-a < y < a$, three sets of boundary conditions are designated as follows:

full constraint:
$$x = \pm a, \quad u = 0$$
$$\tau_{xy} = 0$$
$$y = \pm a, \quad v = \pm v_o$$
$$\tau_{xy} = 0$$

Poisson constraint:
$$x = \pm a, \quad u = \mp \nu v_o$$
$$\tau_{xy} = 0$$
$$y = \pm a, \quad v = \pm v_o$$
$$\tau_{xy} = 0$$

nil constraint:
$$x = \pm a, \quad \sigma_x = \tau_{xy} = 0$$
$$y = \pm a, \quad v = \pm v_o$$
$$\tau_{xy} = 0$$

where (u,v) are the displacement components in the (x,y) frame, and σ_x, τ_{xy} are stress components. Several detailed matters deserve comment. No shear loading is included, the effect of shear being in some measure taken into account by changing orientation of the inclusion-inclusion axis. The prescribed value v_o is meant to indicate an accumulation of displacement as a

result of successive increments of excitation. Thus, $v_o = \Sigma \delta v_o$. Further discussion on this follows. The Poisson constraint corresponds to a plane stress displacement field for the overall domain, although the analysis itself presumes plane strain. In this manner we view the material within the element map as being part of a larger specimen; local behavior, however, is tuned to the fact that the dimensions of the inclusions are relatively quite small.

Material characterization is the third part of the modeling. Ideally, we would prefer to have actual tensile data for the two Ti phases presumed to comprise this model. In practice, however, such information is difficult to obtain and some degree of approximation is virtually unavoidable.* Fortunately, a companion research activity has been in progress, and we were able to obtain suitable representations of the material characteristics from it [8]. The results are shown in Figures 4a and b, and one observes certain differences between the α and β phases of this alloy. Elastically, the α phase (inclusion) is somewhat stiffer, but begins to yield at a lower stress. Once yield initiates, the β phase is noticeably more compliant in that the flatness of the stress-strain curve will allow strain to accumulate rapidly with a very moderate rise in stress. The β phase (matrix) is seen to work-harden to a greater degree and will thereby require greater excitation to reach a point of rapid strain accumulation.

It is thus with some care that the geometry, loading, and material have been described for these computations. Obviously, there is room for eventual improvement in the sense of specializing the analysis to one or more specific cases as in Figure 1. It should be noted, however, that our objective at this stage is to develop a data base whereby more specific and thereby complex

*Note that the computational scheme we use is fully capable of accepting tensile data, subject only to correction for effects of necking, and no curve-fitting is required. It has been remarked elsewhere that this tends to enhance the accuracy of the computations [9.10]

situations may be modeled, analyzed, and understood. Again, the issue here of direct interest is inclusion-inclusion interaction, how it is manifested and best described. And this interest stems from the basic notion that interaction is the mechanism whereby strain localization and associated phenomena jump in size scale from that of a single inclusion to inter-inclusion spacing; it is this event which is believed to allow behavior on a microstructural scale to grow to macroscale proportions.

OUTLINE OF COMPUTATIONAL MECHANICS

The basic approach to the computations has been reported in detail elsewhere [10,11] and a description here need only be brief. Strains are separated into elastic and plastic parts, the first obeying Hooke's law (isotropic). The plastic strains accumulate from increments which are the results of excitation itself being applied incrementally, i.e., in a step-by-step manner. These plastic strain increments are linearly related to the stress increments through a flow rule. Many such flow rules exist, and we have chosen to use the so-called Prandtl-Reuss flow rule which necessarily presumes that the material yields according to the von Mises criterion. Thus if the octahedral stress is given by the general formula

$$\tau_o = \sqrt{[(2/9)(\sigma_x^2 + \sigma_y^2 + \sigma_z^2 - \sigma_y\sigma_z - \sigma_x\sigma_z - \sigma_x\sigma_y + 3\tau_{yz}^2 + 3\tau_{xz}^2 + 3\tau_{xy}^2)]}$$

and, in plane strain, the particular form

$$\tau_o = \sqrt{[(2/9)(\sigma_x^2 + \sigma_y^2 + \sigma_z^2 - \sigma_y\sigma_z - \sigma_x\sigma_z - \sigma_x\sigma_y + 3\tau_{xy}^2)]}$$

we have a basis for measuring the extent of yield or plastic flow. (The usual stress notation is used above.) It is relatively straightforward to demonstrate that the general flow rule is

$$\delta\varepsilon_{ij}^{(p)} = \delta\sigma_{k\ell}s_{ij}s_{k\ell}/6\mu_o^{(p)}\tau_o^2; \quad s_{ij} = \sigma_{ij} - \sigma_{rr}\delta_{ij}/3$$

where δ denotes a small increment in the quantity to which it is attached, and standard indicial notation is employed. Note that the incremental δ is distinct from the Kronecker δ_{ij}. Other notation is described explicitly below. In order to achieve the flow rule for plane strain, the elastic strain increments $\delta\varepsilon_{ij}^{(e)}$ are added to the foregoing expression, and the through-thickness strain increments (i.e., $\delta\varepsilon_{i3}$) are set to zero. The result is, in (x,y)

cartesian coordinates,

$$E(1+s_z^2/s_o^2)\delta\varepsilon_x = [1 - \nu^2 + (s_x^2+2\nu s_x s_z+s_z^2)/s_o^2]\delta\sigma_x$$

$$+ [-\nu(1+\nu) + (s_x s_y-2\nu s_z^2)/s_o^2]\delta\sigma_y + 2[(s_x+\nu s_z)\tau_{xy}/s_o^2]\delta\tau_{xy}$$

$$E(1+s_z^2/s_o^2)\delta\varepsilon_y = [-\nu(1+\nu) + (s_y s_x-2\nu s_z^2)/s_o^2]\delta\sigma_x$$

$$+ [1 - \nu^2 + (s_y^2+2\nu s_y s_z+s_z^2)/s_o^2]\delta\sigma_y + 2[(s_y+\nu s_z)\tau_{xy}/s_o^2]\delta\tau_{xy}$$

$$E(1+s_z^2/s_o^2)\delta\gamma_{xy} = 2[\tau_{xy}(s_x+\nu s_z)/s_o^2]\delta\sigma_x + 2[\tau_{xy}(s_y+\nu s_z)/s_o^2]\delta\sigma_y$$

$$+ 2\{(1+\nu) + 2[\tau_{xy}^2 + (1+\nu)s_z^2]/s_o^2\}\delta\tau_{xy}$$

where

$$s_x = (2\sigma_x-\sigma_y-\sigma_z)/3$$

$$s_y = (2\sigma_y-\sigma_z-\sigma_x)/3$$

$$s_z = (2\sigma_z-\sigma_x-\sigma_y)/3$$

$$s_o^2 = 6\tau_o^2\mu_o^{(p)}/E$$

$$\mu_o^{(p)} = \mu_o^{(p)}(\tau_o) = d\tau_o/d\gamma_o^{(p)}$$

Two further considerations now are incorporated. The strain increments relate to the displacement increments

$$\delta\varepsilon_x = \partial\delta u/\partial x, \qquad \delta\varepsilon_y = \partial\delta v/\partial y$$

$$\delta\gamma_{xy} = \partial\delta u/\partial y + \partial\delta v/\partial x$$

which is tantamount to restricting the process to infinitesimal strains, operationally limiting the analysis to accumulated strains of several percent. Second, the full flow rule is inverted to give stress increments in terms of strain increments, viz.

$$(1+\nu)\delta\sigma_x/E = [(1-\nu)/(1-2\nu) - Qs_z^2/s_o^2]\delta\varepsilon_x + [\nu/(1-2\nu) - Qs_xs_y/s_o^2]\delta\varepsilon_y$$
$$- [Qs_x\tau_{xy}/s_o^2]\delta\gamma_{xy}$$

$$(1+\nu)\delta\sigma_y/E = [\nu/(1-2\nu) - Qs_ys_x/s_o^2]\delta\varepsilon_x + [(1-\nu)/(1-2\nu) - Qs_y^2/s_o^2]\delta\varepsilon_y$$
$$- [Qs_y\tau_{xy}/s_o^2]\delta\gamma_{xy}$$

$$(1+\nu)\delta\tau_{xy}/E = - [Q\tau_{xy}s_x/s_o^2]\delta\varepsilon_x - [Q\tau_{xy}s_y/s_o^2]\delta\varepsilon_y + [1/2 - Q\tau_{xy}^2/s_o^2]\delta\gamma_{xy}$$

where

$$1/Q = (1+\nu)(1+\mu/\mu_o^{(p)})$$

and we require that the stress increments be equilibrated against one another and external loads. Without writing the result in detail, it should be evident that the basic requirements of kinematic compatibility, material behavior, and equilibrium are all fully incorporated.

An analytic solution to these equations is unattainable except in the simplest of cases, *e.g.*, pure bending of a beam. We therefore revert to computational techniques, and the finite element method is most attractive in its ability to accommodate the geometry involved, plus other features indicated below. Basically, the method works as follows. The domain of interest is modeled by a large number of small pieces - called elements - connected at well defined points - called nodes. Each element is permitted to deform in a prescribed manner, e.g., linear distribution of the (incremental) displacements. The corresponding (incremental) strains are computed and, using an analogue to the theorem of minimum potential energy, one determines the (incremental) forces at the nodes required to maintain external equilibrium and the internal strains. These forces will depend upon the degree of yield in that the material is increasingly compliant as it goes further along the stress-strain curve. The relationship between the incremental displacements

and incremental forces is linear, in that the flow rule relating incremental strains and stresses is linear, and this relationship is algebraic rather than in terms of derivatives. Using finite elements, the requirement to solve complicated differential equations is therefore replaced by a need to solve a set of linear algebraic equations.

All that is left is to perform the computation successively in a manner such that (a) the material tracks its own stress-strain curve, and (b) internal strains and stresses accrue as external excitation builds. We have devised computational procedures to perform this task which prove to be efficient and accurate [9,10]. It is these techniques which have been used in the present work, and the computational results are believed to be of the same calibre as those reported in other efforts.

COHERENT MODEL

From the standpoint of developing an initial baseline of data, the simplest problem class to consider is that in which the material is fully coherent. That is to say, no flaws, fissures, or other discontinuities exist within the domain under analysis, Figures 3a-3e. While of course this does not represent fully the range of metallurgical observations, it nonetheless provides an indication of the effect of inclusions *by themselves*; we also have a basis for evaluating the influence of alternate models.

We have therefore performed the following initial computation. Assuming full coherence of the material, excitation was applied in terms of displacements as indicated above, using the following scheme. The initial "load" increment necessarily elicits (linear) elastic response, and its magnitude is scaled to bring the most highly stressed element just beyond the brink of yield. The next increment is adjusted to be 5 percent of the first, the third is 5 percent of the accumulated sum, and so on. A total of 25 "load" increments was applied.

This procedure was followed for each of 15 cases, involving five orientations of the inclusion-inclusion axis and three types of lateral constraint. Since the constraint affects the magnitude of excitation required to initiate yield,* the final level of excitation was different for each of the three types of lateral constraint. For reference we list them below in terms of the (vertical) axial strain imposed and the representative octahedral strain level achieved, far from the inclusions. Clearly, excitation was not excessive,

*Orientation of the inclusion-inclusion axis has only a marginal effect on this, owing to the smallness of the inclusions.

	accumulated v_o/a	representative value of accumulated γ_o/γ_{1im}
full constraint	0.0322	2.48
Poisson constraint	0.0270	2.46
nil constraint	0.0252	2.87

but did reach a level [illegible] entire field had yielded. Since the strain values shown refer to [illegible] material, it is clear by comparison to Figure 4b that this phase had rounded the knee of the stress-strain curve but did not reach the point where strain could accumulate rapidly with only minor increase in stress level. The same is not true of the α phase.

The results* are interesting in several respects. Throughout the excitation cycle, the stress and strain fields in the α phase showed very little directional character, for all orientations of the inclusion-inclusion axis. The one distinguishing characteristic of the response interior to the inclusion was a high degree of hydrostatic tension accompanying the yield process. Typically, the hydrostatic stress was 4-14 times the yield stress of the α phase. We return to the implications of this information below.

In the matrix material, near the α-β interface, response was both directionally oriented and mixed. On the right and left sides** of the inclusions, stress tended to concentrate just as might be expected from classical analysis of the related problem of a hole in a plate under tension [6]. Above and below the inclusions, however, strain tended to concentrate. One must be more specific in making these statements, however, to avoid misinterpretation. The stress concentration on the sides of the inclusion is in terms of a hoop stress, just as is used to gauge the effect of a hole in a classical elastic stress analysis. Owing to the presence of the inclusion,

*As a practical matter, we note that each of the 15 computer runs required 16 secs on the Univac 1108, so that cost of these analyses is not excessive.

**Recall that excitation is vertical, constraint lateral or horizontal.

however, and to the hydrostatic state in its interior, the normal stress on the inclusion's sides is important. The combination of the two, plus the through-thickness stress characteristic of plane strain, tends to inhibit growth of the effective or octahedral stress. On the other hand, the strains above and below the inclusion tend to differ by greater amounts, and we observe a relatively larger amount of the type of strain associated with yield. This situation is depicted in Figures 5a to 5e, in which octahedral strain around the inclusion (but measured just within the matrix) is shown for one type of constraint. The four excitation levels correspond to (1) initiation of yield in the inclusion, (ii) initiation of yield in the matrix (far field), (iii) matrix strain roughly equal to the 0.2 percent offset, and, (iv) about twice the third level (achieving the values shown in the table above).

Such is the response in the inclusion and just outside the α-β interface. The question now arises as to whether the influence of the inclusion spreads beyond its immediate vicinity. The answer here is a little disappointing, and we are obliged to stretch the credibility of the numerical data to demonstrate the trend. The expectation is as follows. Once initial concentrations of a given stress component have been relaxed by attendant yield, the zones over which plastic flow should be most pronounced will lie at about ± 45 deg from the direction of excitation. Indeed such behavior is observed and is most apparent in terms of either octahedral or effective strain. We show in Figures 6a-6e an inference of this behavior, having darkened those elements for which γ_o/γ_{lim} is at least 1 percent greater than the far field value. The trouble, however, is that the elevation of this strain - relative to the far-field value - is small, and one is somewhat pressed to use such information as a meaningful guide. It is nonetheless

true that the greatest tendency for interactions between inclusions occurs when their connecting axis is at ± 45 deg to the vertical and, moreover, both octahedral and effective strains appear to be the most sensitive measures of this effect.

Hence we are able to make limited inferences as to response of the coherent model at modest levels of excitation. What information can be extracted from the computational results is nonetheless consistent with expectation, at least on the basis of the problem's mechanics, but the behavior is less definitive than might be hoped.

BURST MODEL

Since one of the major features of the coherent model is the high hydrostatic tension within the inclusion, it is natural to create a second model which responds to this information in a suitable manner. Were we to proceed solely on the basis of microstructural observation, debonding at the α-β interface would be the obvious extension to the coherent model. From the standpoint of the analysis, however, this has a serious drawback and we again prefer a more cautious approach.

The difficulty lies in choosing the region of debonding, and it is conceptual. One must in some manner decide

- the position along the interface where debonding occurs
- the extent (length) of the debonded interface
- the timing within the excitation cycle when debonding takes place.

In effect one is asked to insert a micro-fracture criterion, and then to separate out its influence from other factors. Pursuing such a course is clearly in conflict with our objective at this stage, to utilize computational mechanics to infer such information. Subsequent work will address these matters.

Accordingly, we have chosen to allow the inclusion to burst from within, i.e., to let the interior open up. This has the overall effects of relieving the hydrostatic tension which otherwise builds up, and of making the inclusion - taken as a piece - considerably more compliant. The non-directionality of the inclusion's apparent *properties* is preserved and, while this type of behavior may not be frequencly observed, the essential feature of relaxing inclusion-matrix integrity is in some measure replicated.

We remark in passing that such alteration is altogether straightforward in finite element analysis; one need only modify the connectivity of the elements rather than construct a new element map from the outset.

With this modification, the type of analysis described above was repeated. For comparison, we record the final levels of excitation for the three types of lateral constraint.

	accumulated v_o/a	representative value of accumulated γ_o/γ_{lim}
full constraint	0.0181	1.40
Poisson constraint	0.0177	1.62
nil constraint	0.0165	1.76

It is to be observed that considerably lower levels of excitation initiated plastic flow for all types of constraint, in that the final excitation levels are less than in the coherent model, even though the same algorithm for step sizing and the same number of steps were used in the computations.

The results, too, are quite different. We show first the angular distribution of octahedral strain for each of the inclusion-inclusion axis orientations, and for each of the types of constraint in Figures 7a to 7e, 8a to 8e, and 9a to 9e. Whereas the coherent model (Figures 5a-5e) showed a fair degree of angular sensitivity, the effect now is magnified. Moreover, the strains achieved can greatly exceed those for the coherent model even though far-field excitation is lower by nearly half.

It is also evident that the regions of highest (octahedral) strain concentration have shifted from positions above and below the inclusions to ones which are roughly on the right and left sides. These sites are not distinctly positioned for all cases (see, e.g., Figure 7e), and range from a narrow part of the interface to a fairly extensive region along the interface. (Compare,

e.g., Figures 8e and 9b.) In viewing these figures, it is evident that the data tend to be noisy in some respects; while we acknowledge this behavior, we recognize also that the maps are not of a nature to accommodate the high gradients that occur in certain of these results. Nonetheless the sense of the data is taken to be acceptable, and we proceed to draw certain conclusions from the sets of Figures 7, 8, and 9.

It is clear that the magnitude of peak values of γ_o/γ_{lim} is quite sensitive to lateral constraint, with the greatest values occurring at the greatest constraint. (Note the change in scale between Figures 5a-5e and 7a-7e, et seq. In the latter, data are shown only for the highest "load" level. It is Figures 9a-9e that compare directly to the upper values in Figures 5a-5e.) Whereas, in the coherent model, maximum and minimum values of γ_o/γ_{lim} are about +20 per cent and -10 percent of the far-field level, the burst model shows very different behavior. Maxima are several times the far field level of γ_o/γ_{lim} (exceeding 8x in some instances), and minima are below yield. Clearly, we have evidence of strain localization in these data alone. Of further interest, tendency of interaction is enhanced by constraint. Looking, for example at Figures 7d, 8d, and 9d, it is observed that the presence of a neighboring inclusion affects the relative magnitude of peak strains at this excitation level in a manner that reflects the growing degree of constraint among the three cases. Finally, and somewhat of a surprise, the degree of interaction - as inferred from relative peaks in γ_o/γ_{lim} is roughly is proportion to the angle of the inclusion-inclusion axis. This suggests that over-and-under inclusions are virtually unaffected by one another, whereas side-by-side configurations would tend toward much higher degrees of interaction, at least to judge from behavior at the matrix-inclusion interface. Information presented below modifies this inference, but the

pattern of strain localization and its sensitivity to parameters included in this study are nonetheless distinct.

Not shown, but apparent from the numerical printout, are two further points. The hydrostatic stress within the inclusion has been reduced which, after all, was the intent of this exercise. In addition, a considerable degree of angularity in the magnitude of yielding within the inclusion is to be seen.

Finally, we examine the tendency of higher strains at one inclusion to reach outward and thereby to interact with strains at the neighboring inclusion. Here we need not stretch the numerical data, as in the coherent model. It is relatively simple to identify those elements for which the octahedral strain exceeds 5 per cent and 10 per cent of the far-field value; the corresponding sketches are shown in Figures 10a-10e, 11a-11e, and 12a-12e. The shapes of the resulting zones are somewhat different for the 0 and 90 deg orientations of the inclusion-inclusion axis, relative to Figures 6a-6e; otherwise, some similarity is to be noted. In addition, we observe that, apart from the 0 and 90 deg orientations, sensitivity to constraint is modest. What does emerge most clearly is the degree to which the two inclusions tend to interact over the space separating them. In all cases the larger plastic strains tend to reach outward at about $\pm$ 45 deg to the line of loading so that, in the case where the inclusion-inclusion axis itself is at 45 deg, these zones of higher plastic strain actually connect; see Figures 10c, 11c, and 12c. Such is not the case for other orientations so that the intense strain localization indicated in Figures 9a to 9e is effective in promoting interaction only when other conditions permit. Indeed, this point is borne out by the pattern in Figures 10a-10e. Although strain localization at the interface is much less intense, connectivity of the higher strain zones is still to be seen in Figure 10c.

In this model, the inclusion is made much more compliant than in the coherent case and, as a result, we see that the strains in the matrix (near the interface) can become dramatically increased. This behavior can be confined to a small portion of the interface region or it may be spread out, depending on external factors which, frankly, is a little surprising. Even so, the tendency for these intense strains to spread and thereby to interact with those emanating from another inclusion appears to depend primarily on the relative location of that other inclusion and only to a lesser degree on other factors. To the extent that the computation is directed toward identifying those features which lead to inclusion-inclusion interaction, the data presented and discussed in this section are revealing, and the results prompt further and more detailed analysis.

CONCLUDING REMARKS

It is clear that the question of strain localization, posed in terms of inclusion-inclusion interaction, may be addressed with existing computational techniques. With some care in modeling, one need not generate excessive strain levels nor encounter gradients which press computational methods greatly beyond the extremes of their capability. What we have done here is follow this route for two simple cases, proceeding with caution in the modeling process. While some of the analyses produced higher gradients than were anticipated, the results remain credible.

The observations to be made are that inclusion-inclusion interaction will develop, given a reasonable set of circumstances, and that the process can be quite rapid in what is otherwise an innocuous setting. Accounting for plastic flow, however, is a critical part of the overall approach, in that linear elastic analysis would not presage the type of behavior observed here.

Inferentially, the quantitative details will depend upon inclusion-inclusion spacing - we have chosen a large value in this work - and upon relative material properties. One could of course test these parameters but the computational cost rapidly grows large.

More specifically, we have shown that the response within a given model is sensitive to both orientation of the inclusion-inclusion axis, relative to the direction of loading, and to the type of lateral constraint imposed. Of these two parameters, the first indicates which of a set inclusions will "find" and another; the second influences the rate of the attendant process, perhaps owing to the intensity of strain local to the interface.

As a result, we deduce that the next steps in this program of research will involve improvements to the model, emphasis being given to the following items:

- more accurate material data;
- more likely break-up of the inclusion, including debonding with the matrix to create potential voids;
- initiation of voids elsewhere within the matrix owing, perhaps, to sub-micron inclusions, grain boundaries, and other features of real materials; and
- tracking the growth of these voids.

Two methods for pursuing this effort are evident. One is to utilize specific experimental data directly, i.e., forcing the analysis to follow a pre-arranged track. It is a happy circumstance that the simple finite elements we employ allow this. The other would involve one or more of several likely local failure criteria, e.g., maximum tensile or octahedral strain or stress, and to determine which gives the most meaningful result in terms of experimental observation. We shall consider both, the end being to move toward creation of a computational simulation of experiment.

ACKNOWLEDGMENT

One of the exciting aspects of this work is the opportunity to begin assimilating unfamiliar kinds of technology in order to adapt existing methods of analysis to new problem areas. We are most fortunate in this respect to have had the counsel of three outstanding physical and mechanical metallurgists at CMU, and wish to thank Professors J. R. Low, Jr., A. W. Thompson, and J. C. Williams for their continuing interest in this work. Professor Low has recently retired from academic life, but we look forward to our association with Professors Thompson and Williams as this research is carried forward.

REFERENCES

1. T. B. Cox and J. R. Low, Jr., An Investigation of the Plastic Fracture of AISI 4340 and 18 Nickel-200 Grade Maraging Steels, *Metallurgical Transactions*, 5 (1974) 1457-1470.

2. A. W. Thompson, Particle Spacings in Ductile Fracture, *Metallurgical Transactions*, to appear.

3. D. M. R. Taplin (editor), *Fracture 1977*, University of Waterloo Press, volume 2: Physical Metallurgy and Voids, Cavities, Forming (1382 pp).

4. D. C. Drucker, The Continuum Theory of Plasticity on the Macroscale and the Microscale, *Journal of Materials*, 1 (1966) 873-910; T. W. Butler, Fracture of WC-Co From a Continuum Viewpoint, *Engineering Fracture Mechanics*, 4 (1972) 487-498; T. W. Butler and D. C. Drucker, Yield Strength and Microstructural Scale: A Continuum Study of Pearlitic Versus Spheroidized Steel, *Journal of Applied Mechanics*, (1973) 780-784.

5. J. R. Rice, The Localization of Plastic Deformation, Theoretical and Applied Mechanics, *Proceedings of the 14th IUTAM Congress*, Delft, The Netherlands, 30 August - 4 September 1976, W. T. Koiter ed. North-Holland Publishing Company, (1976) 207-220.

6. R. E. Peterson, *Stress Concentration Factors*,, John Wiley and Sons, New York (1974) 173.

7. C.-B. Ling, *Journal of Applied Physics*, 19 (1948) 77-82.

8. R. E. Smelser, J. L. Swedlow, and J. C. Williams, Analysis of Local Stresses and Strains in Ti-6al-4V Widmanstatten $\alpha+\beta$ Microstructures, Report SM 76-8a, Department of Mechanical Engineering, Carnegie-Mellon University, April 1977, to appear as ASTM STP.

9. J. L. Swedlow, *International Journal of Fracture Mechanics*, 5 (1969) 25-31; J. H. Underwood, J. L. Swedlow, and D. P. Kendall, *Engineering Fracture Mechanics*, 2 (1971) 183-196.

10. J. L. Swedlow, *Computers and Structures*, 3 (1973) 879-898.

11. J. L. Swedlow, *International Journal of Non-Linear Mechanics*, 3 (1968) 325-336; 4 (1969) 77.

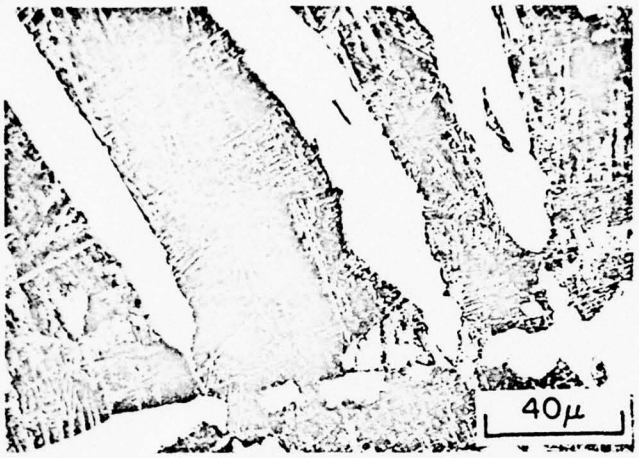

Figure 1. An example of the microstructure used in the present study. Ti-6Al-4V at 500x. Note elongated α particles, or "stringers," in nearly isotropic β matrix. Model is taken to be transverse to longest dimension of particles, hence justifying use of plane strain in analyses; cross-section of particles is taken to be equi-axed.

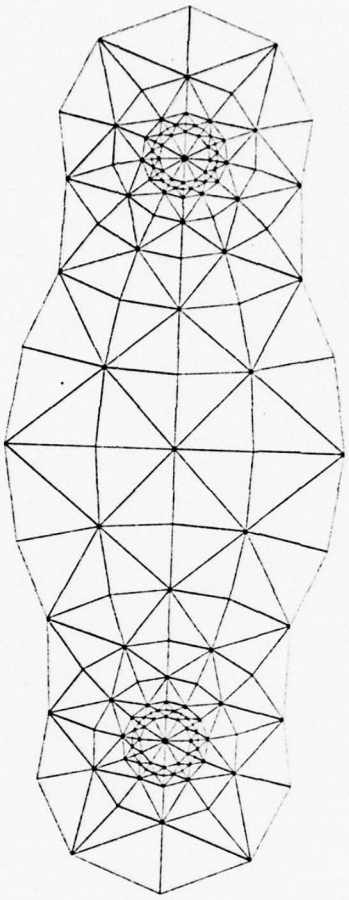

Figure 2. Central region of finite element map showing refinement at α-β interface (through dense regions of elements) and coarsening further away, via use of bipolar coordinates. This array was used in all analyses, as indicated in Figures 3a-3e.

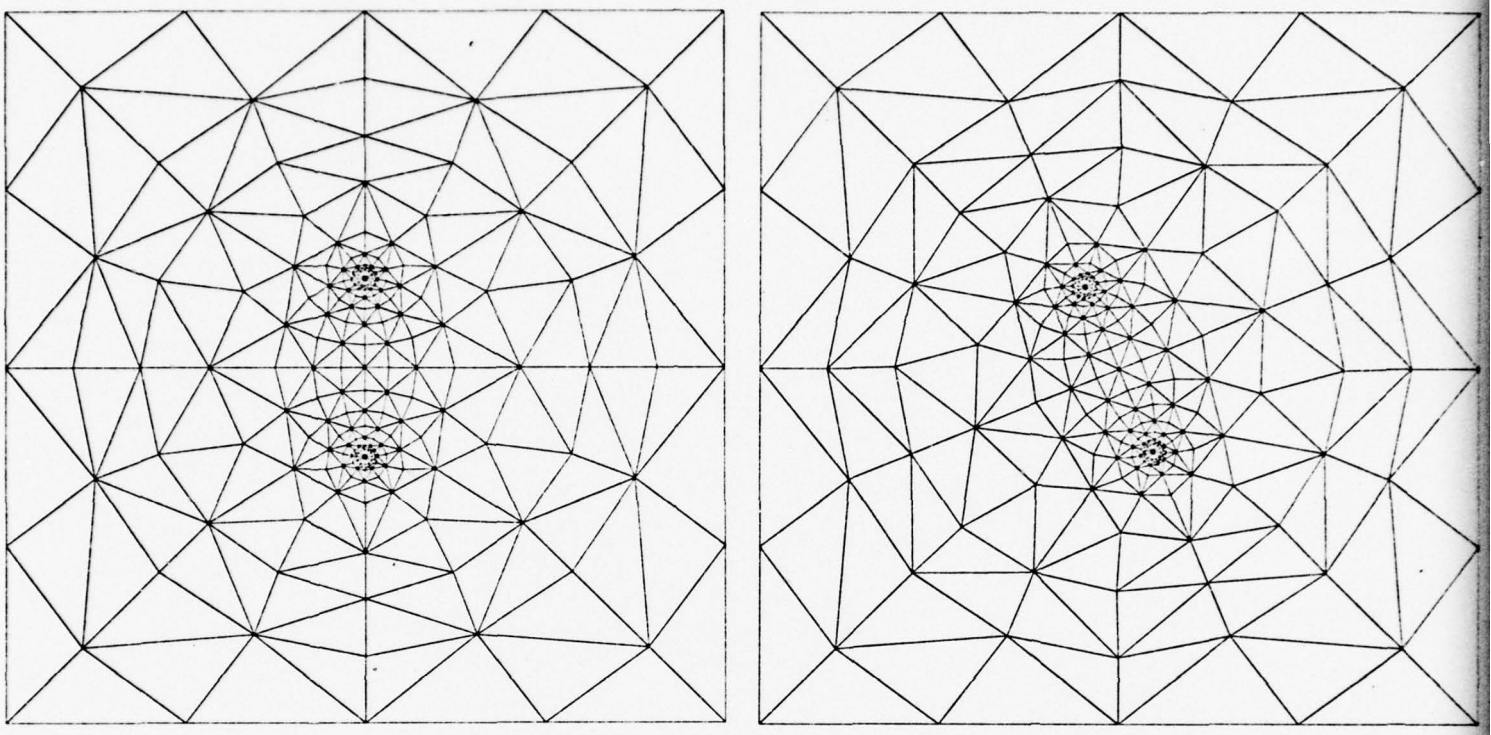

Figures 3a-3e. Element maps used in analyses, showing rotation of inclusion-inclusion axis at 0, 22.5, 45, 67.5, and 90 deg to vertical. Excitation in all cases is vertical, constraint horizontal.

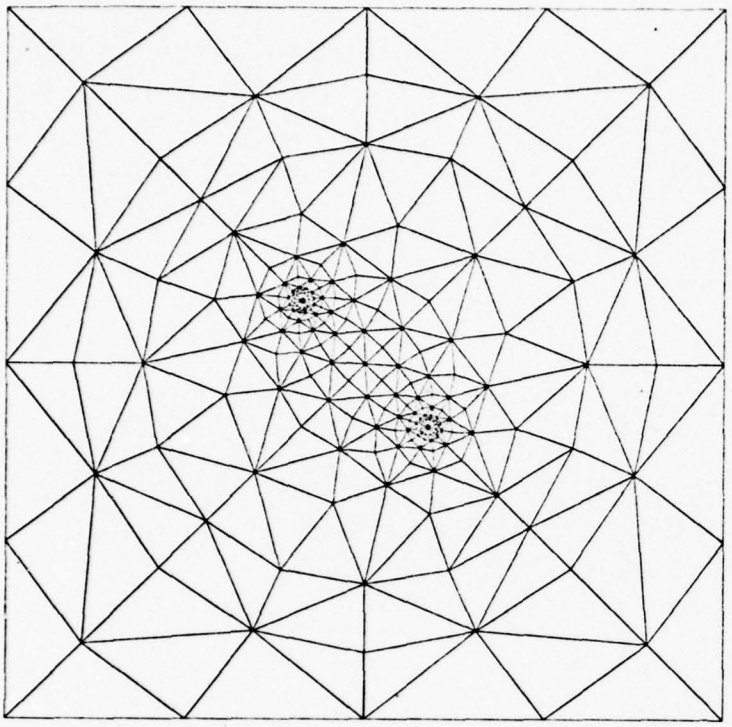

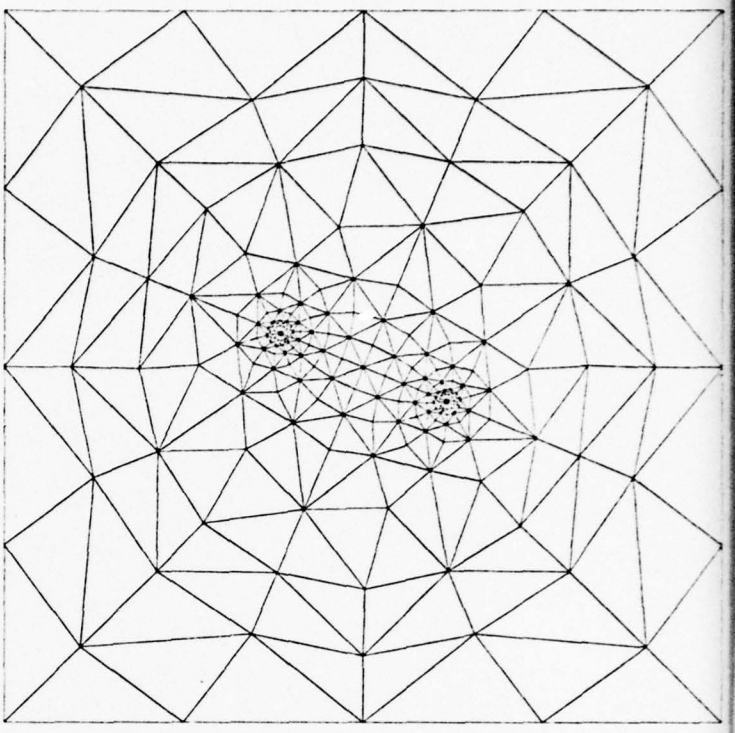

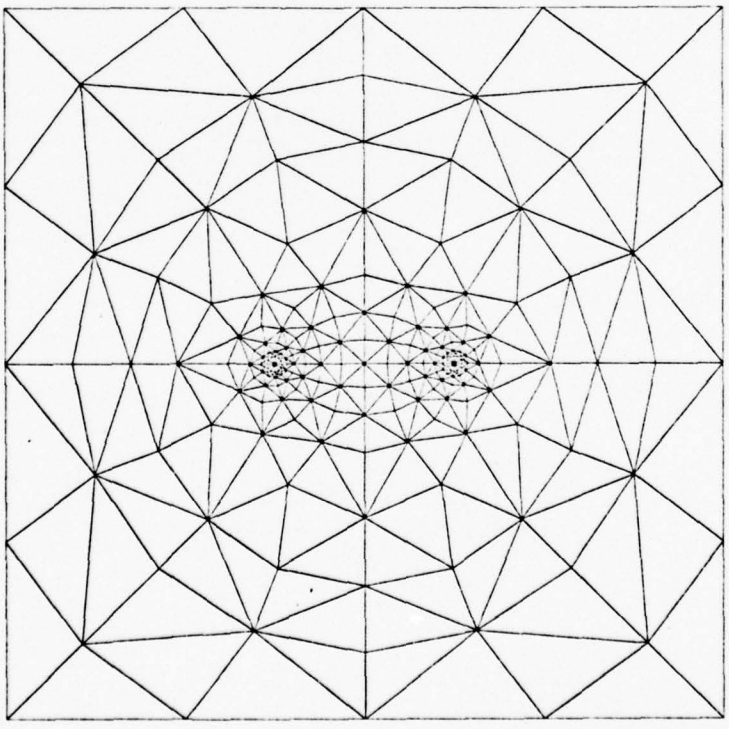

Figure 4a. Presumed stress-strain curve for α phase. $E = 17.5 \times 10^6$ lb/in^2 and $\sigma_{lim} = 115 \times 10^3$ lb/in^2

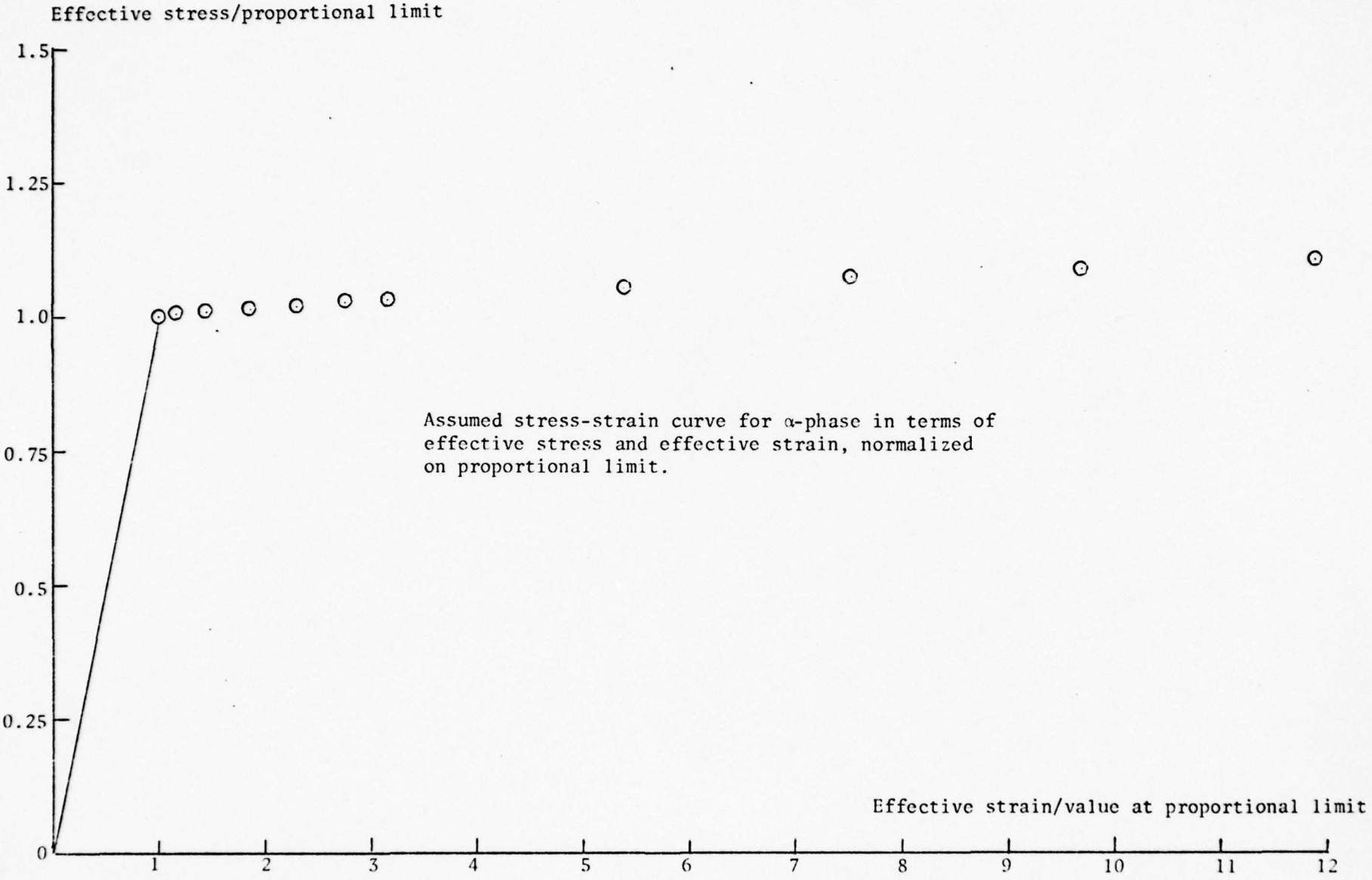

Figure 4b. Presumed stress-strain curve for $_2\beta$ phase.
$E = 13.0\times10^6$ lb/in^2 and $\sigma_{lim} = 130\times10^3$ lb/in^2

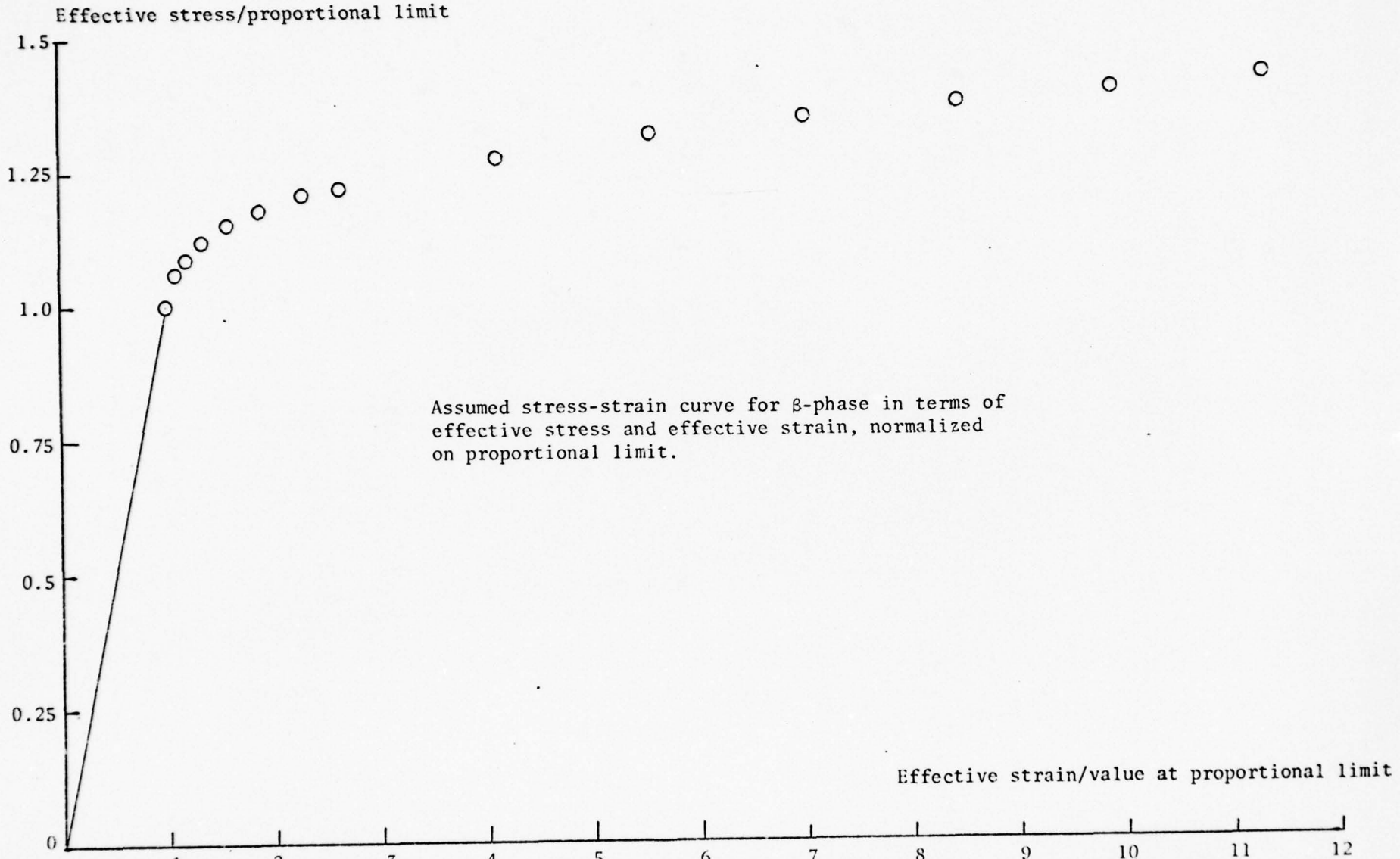

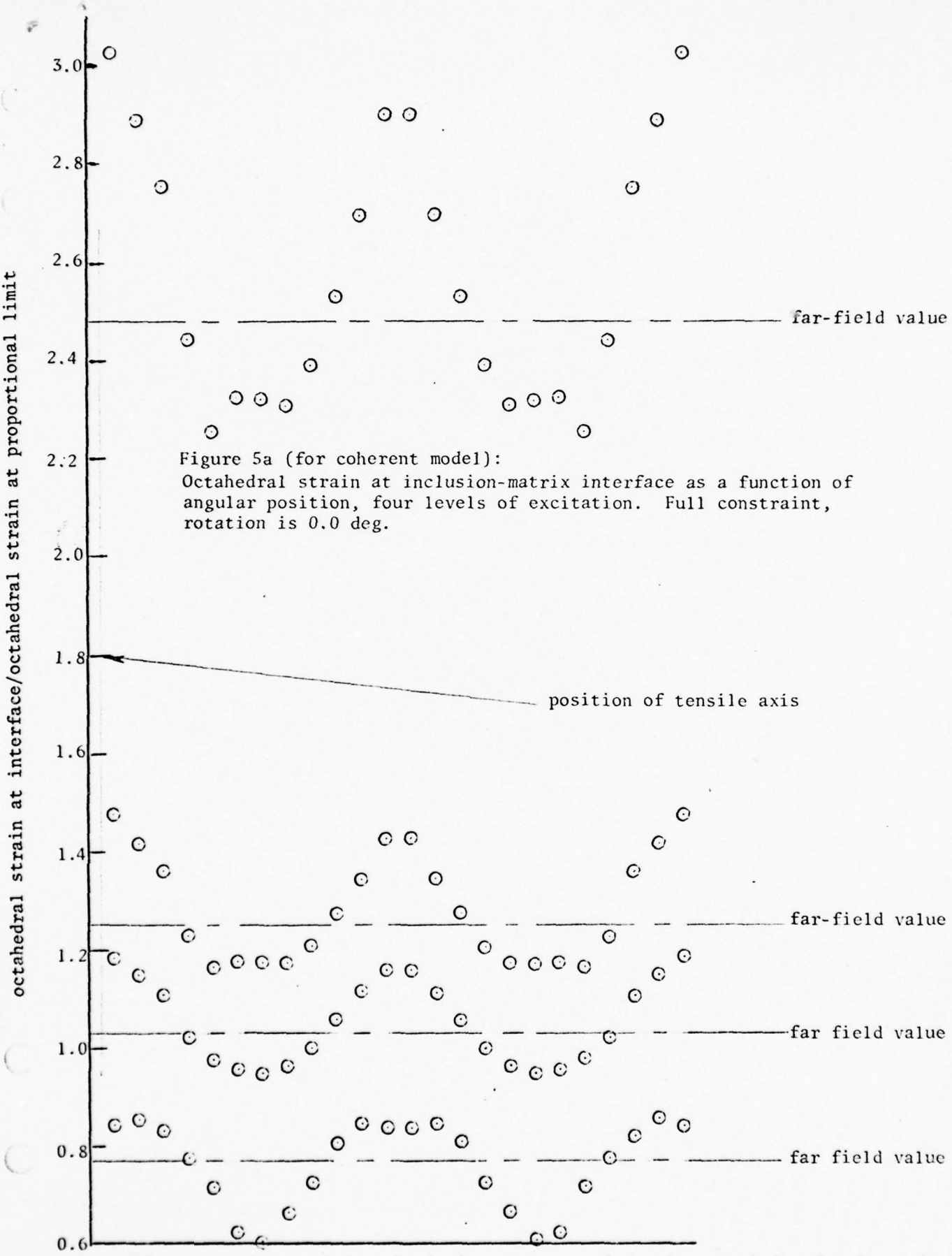

Figure 5a (for coherent model):
Octahedral strain at inclusion-matrix interface as a function of angular position, four levels of excitation. Full constraint, rotation is 0.0 deg.

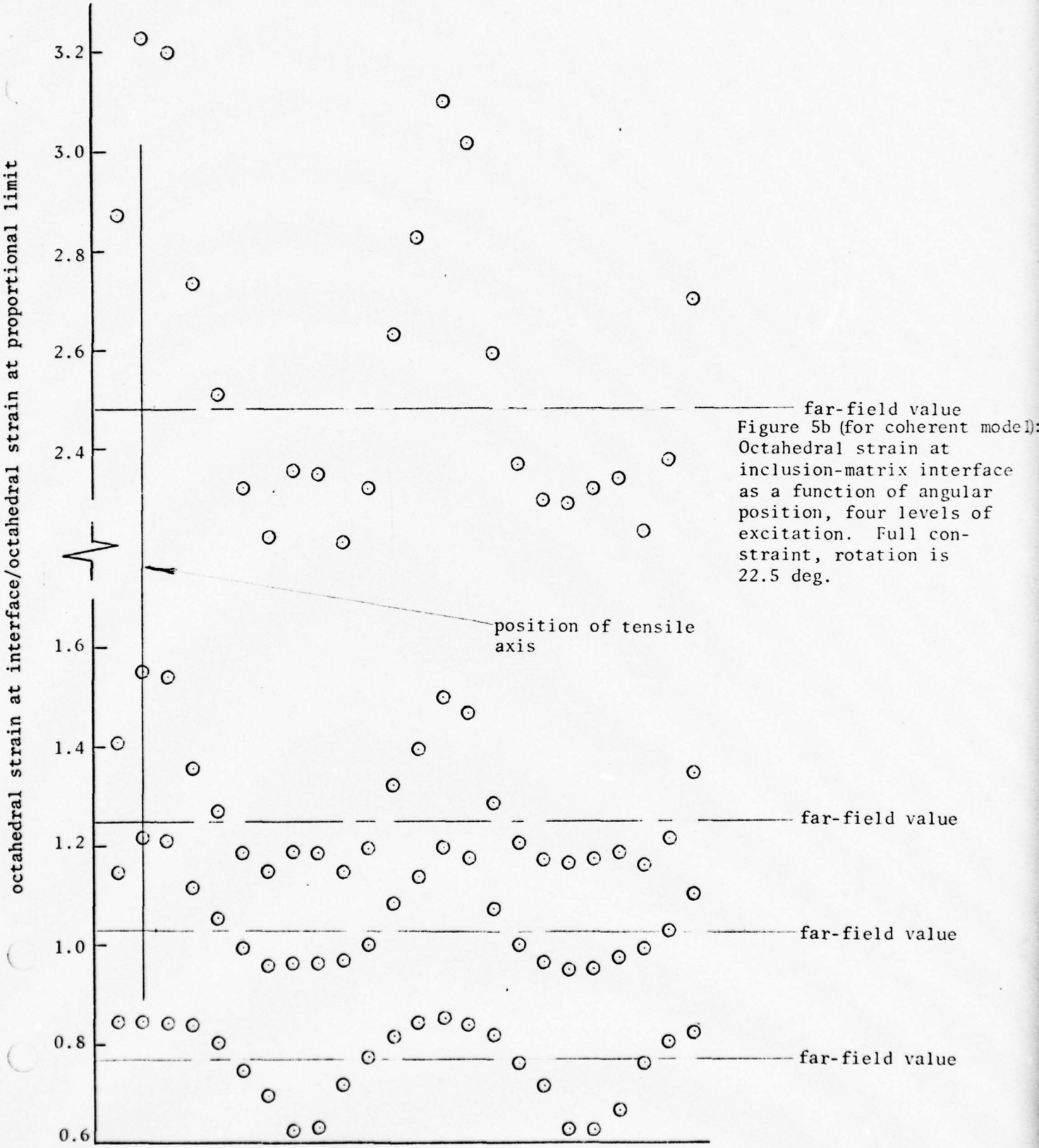

Figure 5b (for coherent model): Octahedral strain at inclusion-matrix interface as a function of angular position, four levels of excitation. Full constraint, rotation is 22.5 deg.

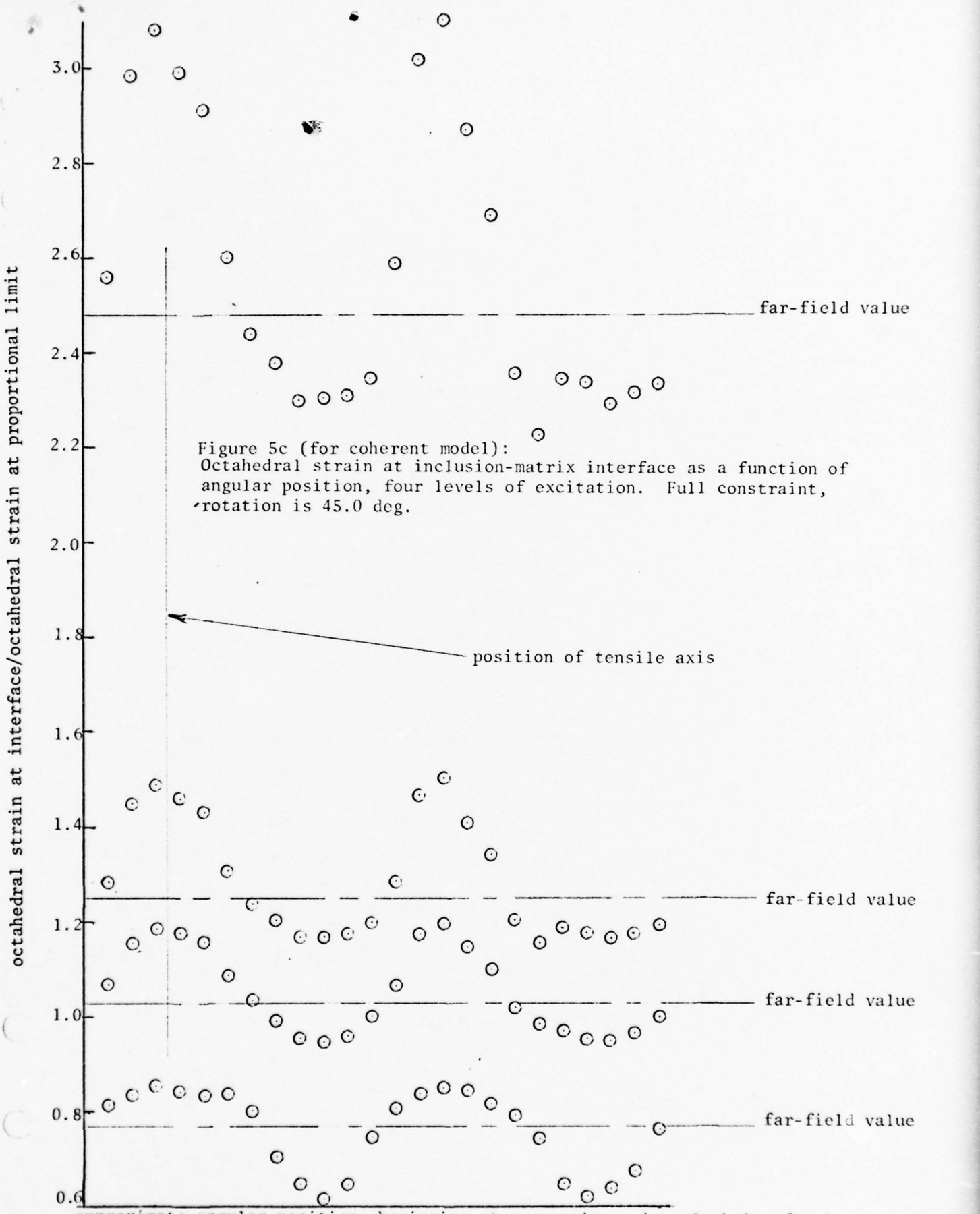

Figure 5c (for coherent model):
Octahedral strain at inclusion-matrix interface as a function of angular position, four levels of excitation. Full constraint, rotation is 45.0 deg.

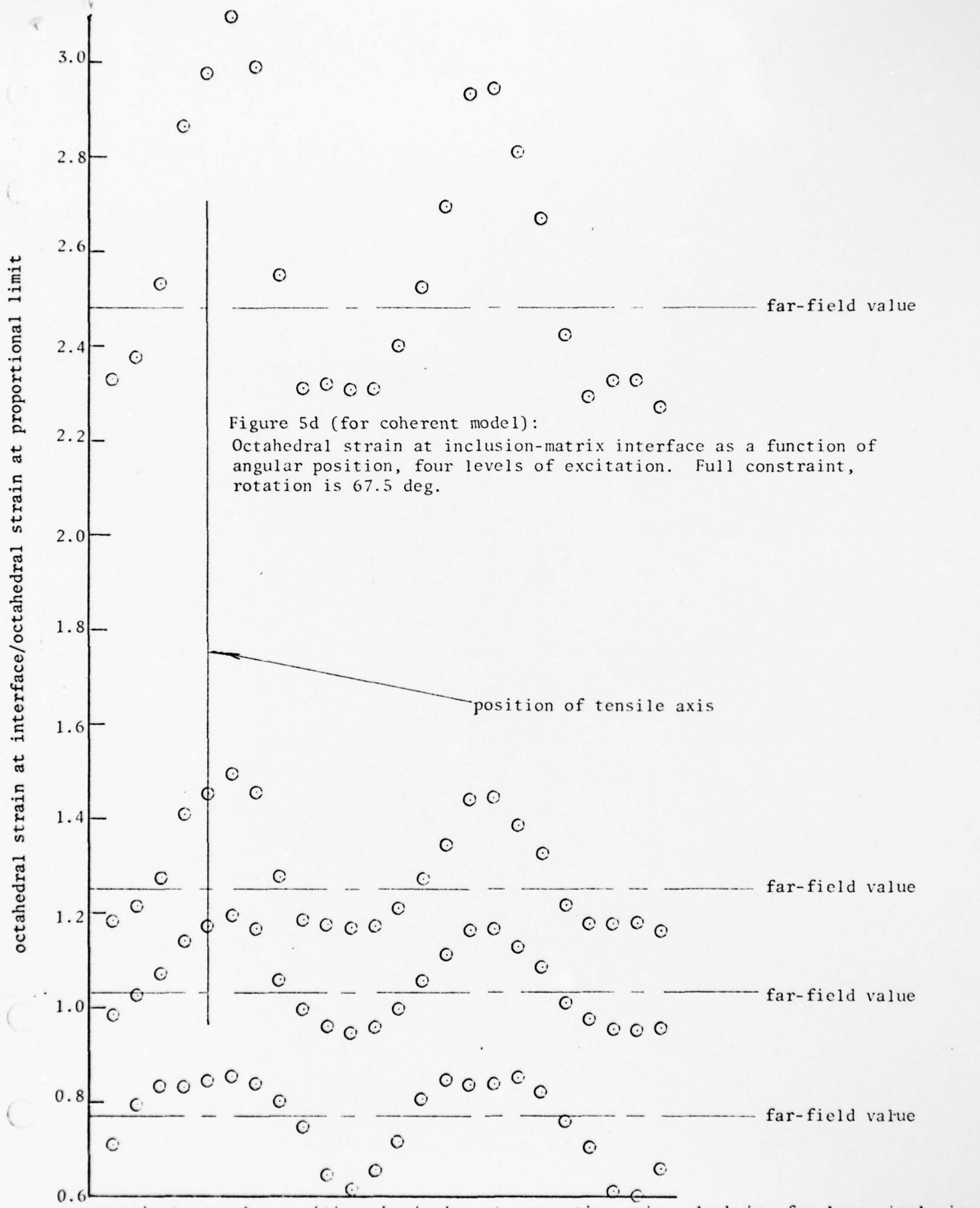

Figure 5d (for coherent model):
Octahedral strain at inclusion-matrix interface as a function of angular position, four levels of excitation. Full constraint, rotation is 67.5 deg.

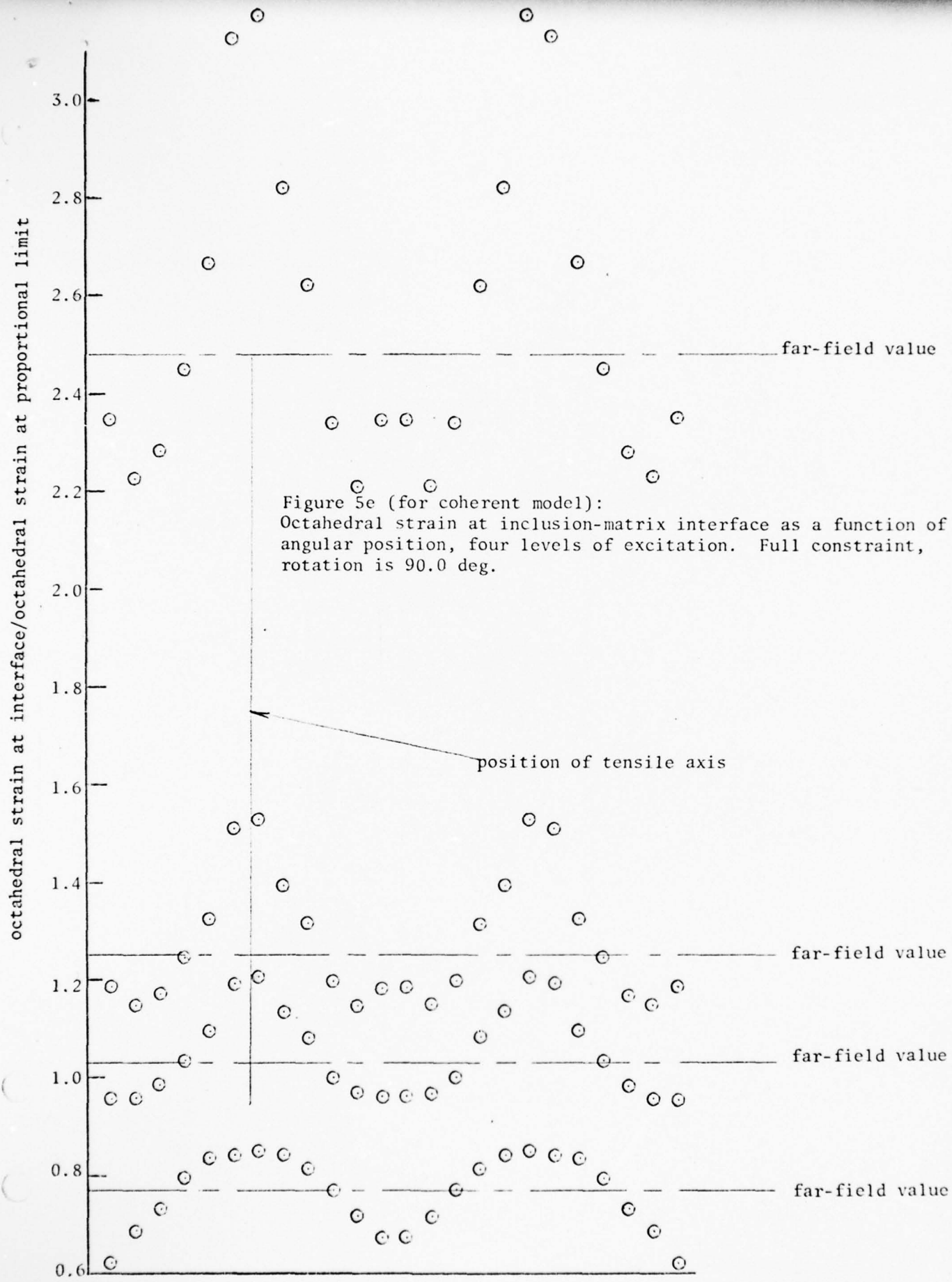

Figure 5e (for coherent model):
Octahedral strain at inclusion-matrix interface as a function of angular position, four levels of excitation. Full constraint, rotation is 90.0 deg.

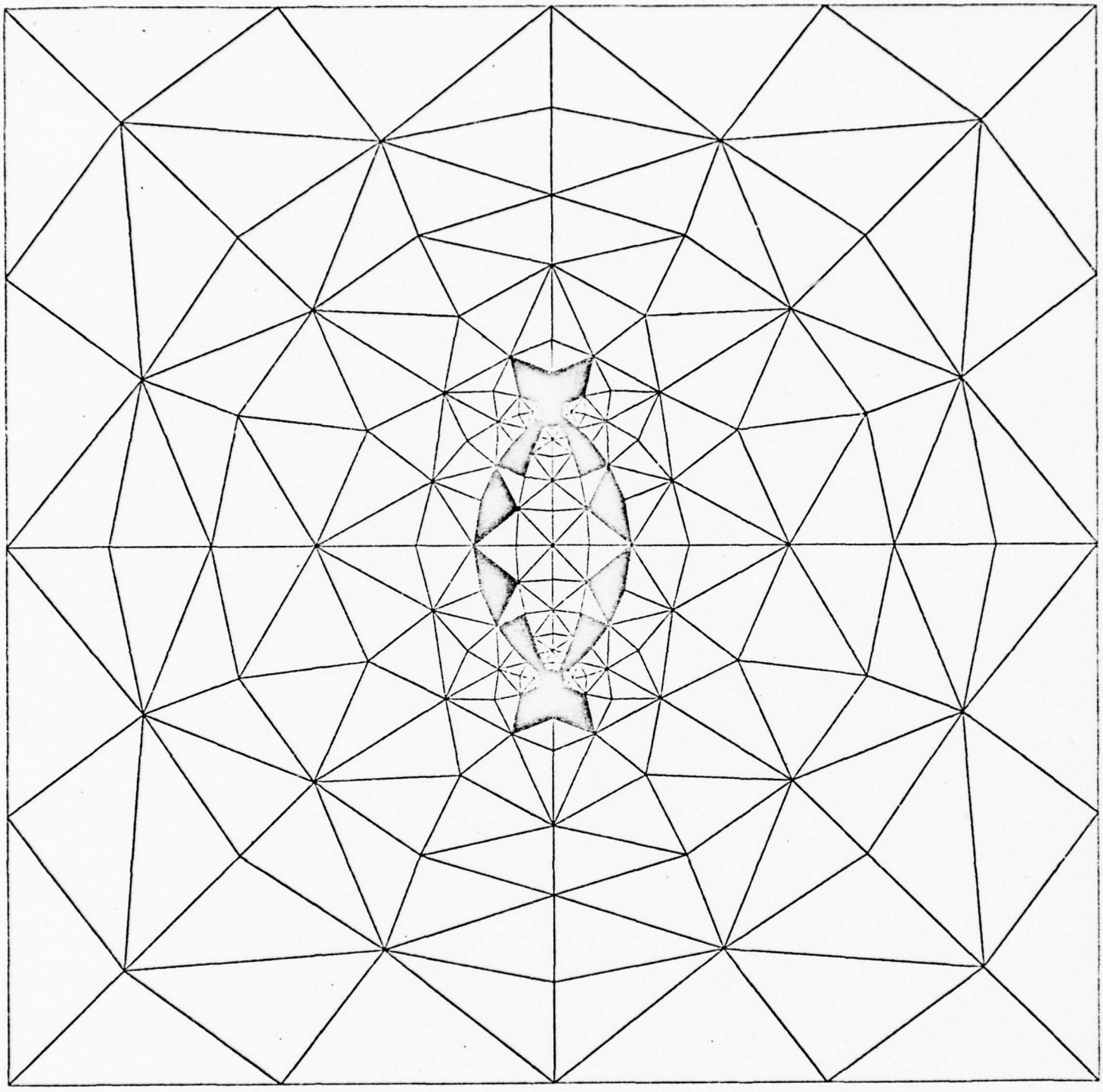

Figure 6a. Regions with greatest propensity for extensive strain, full constraint, rotation is 0.0 deg, coherent model

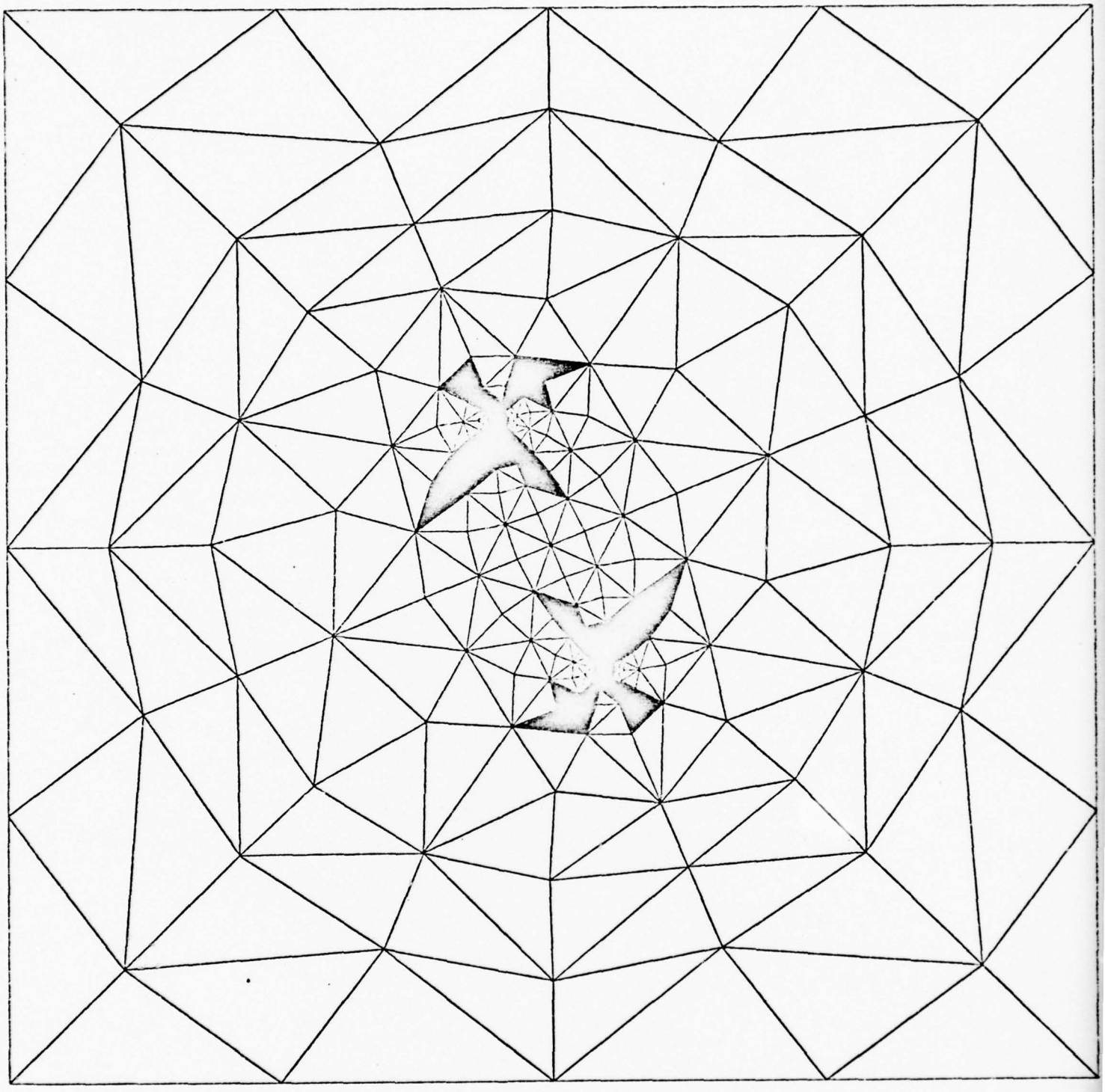

Figure 6b. Regions with greatest propensity for extensive strain, full constraint, rotation is 22.5 deg, coherent model

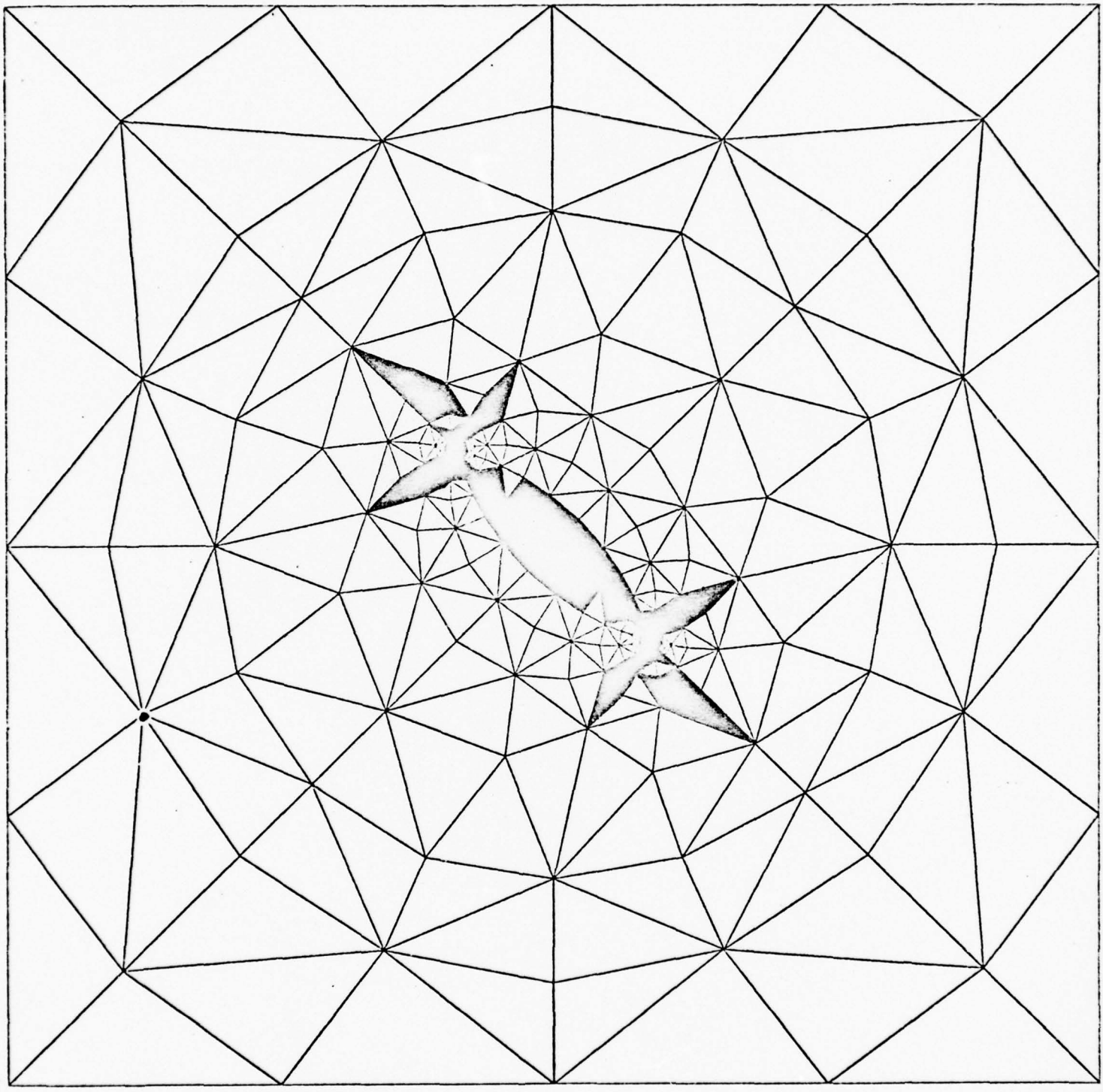

Figure 6c. Regions with greatest propensity for extensive strain, full constraint, rotation is 45.0 deg, coherent model

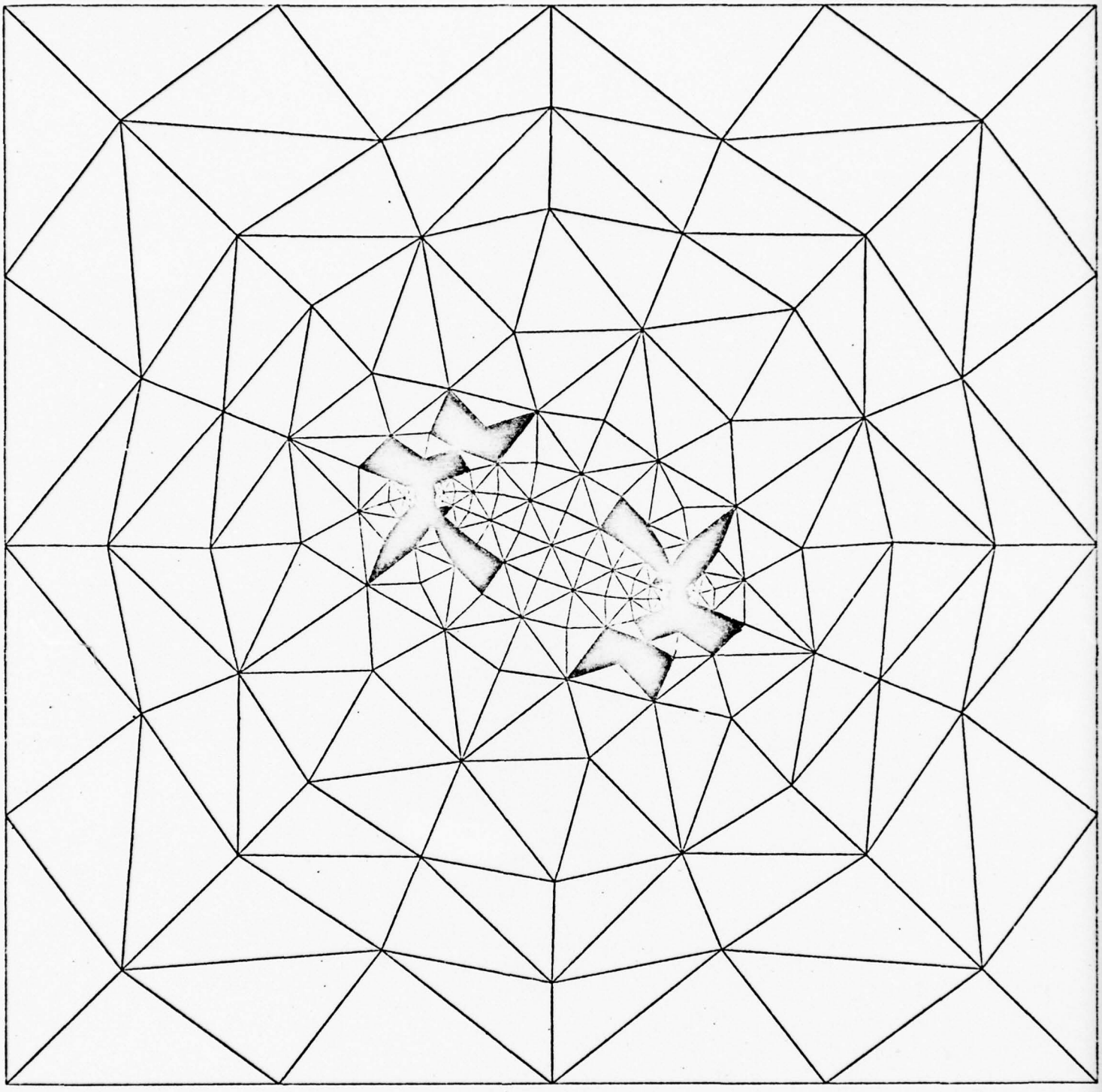

Figure 6d. Regions with greatest propensity for extensive strain, full constraint, rotation is 67.5 deg, coherent model

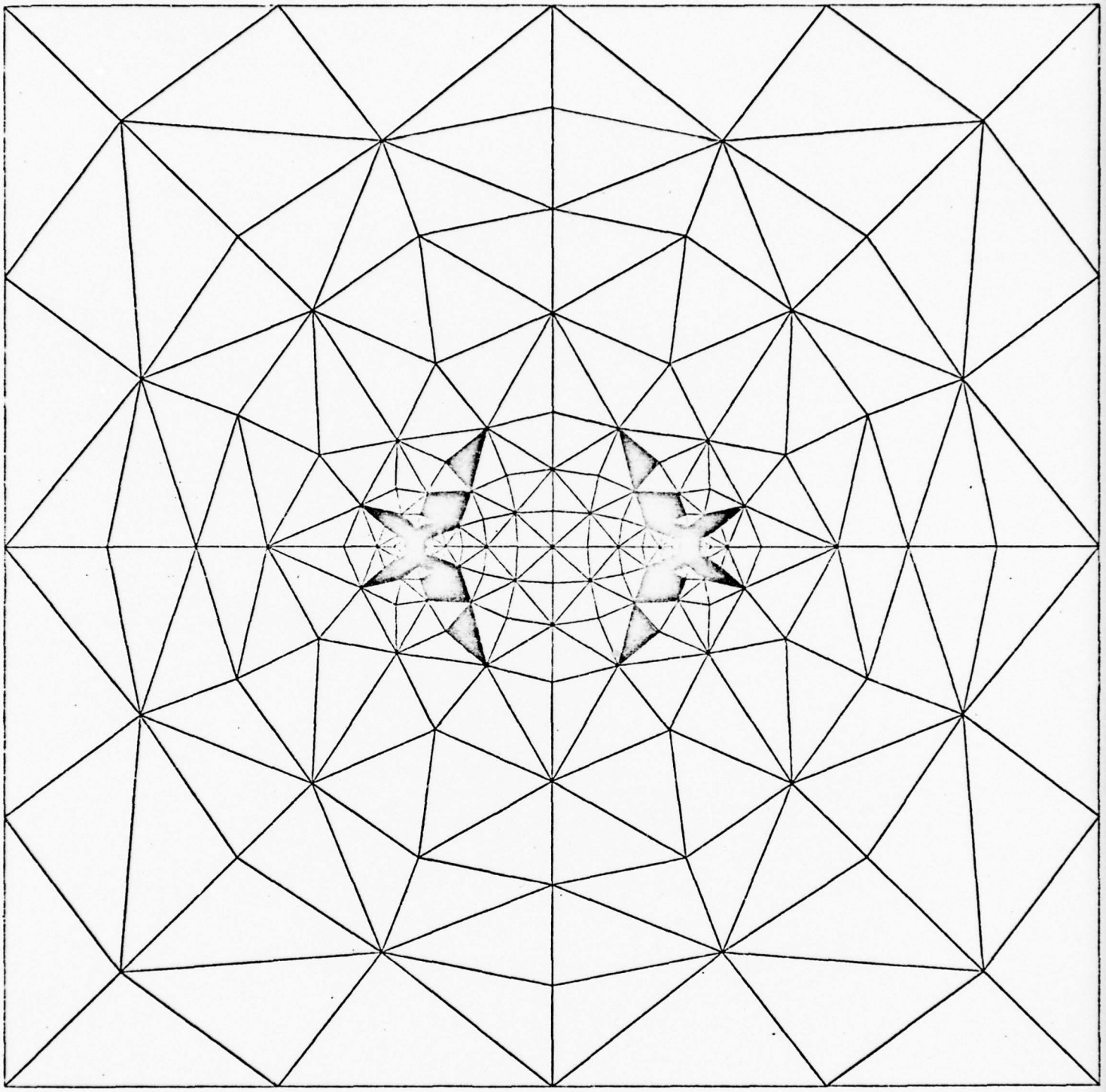

Figure 6e. Regions with greatest propensity for extensive strain, full constraint, rotation is 90.0 deg, coherent model

Figure 7a (for burst model):
Octahedral strain at inclusion-matrix interface as a function of angular position, at highest excitation level only. Nil constraint, rotation is 0.0 deg.

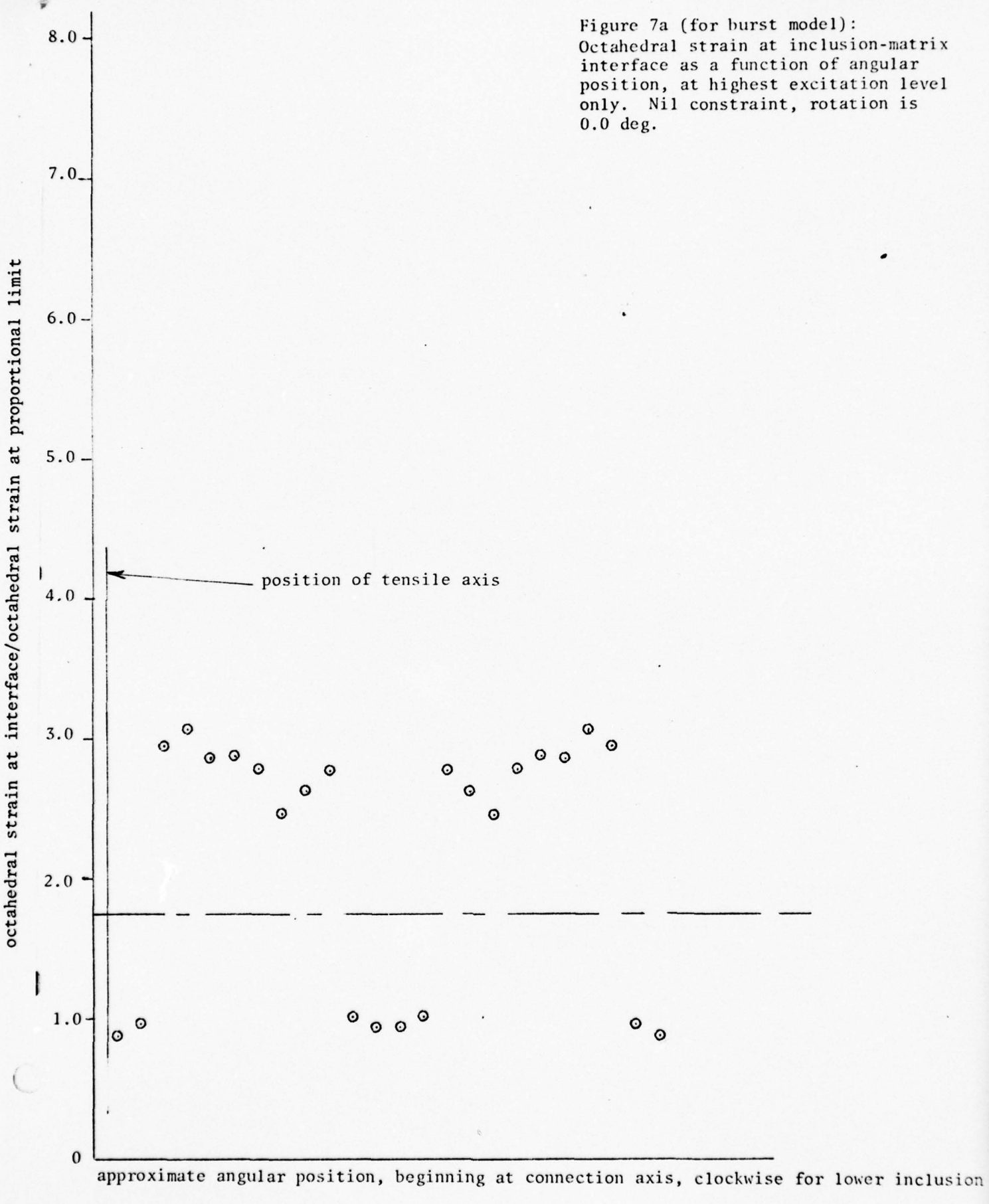

Figure 7b (for burst model): Octahedral strain at inclusion-matrix interface as a function of angular position, at highest excitation level only. Nil constraint, rotation is 22.5 deg.

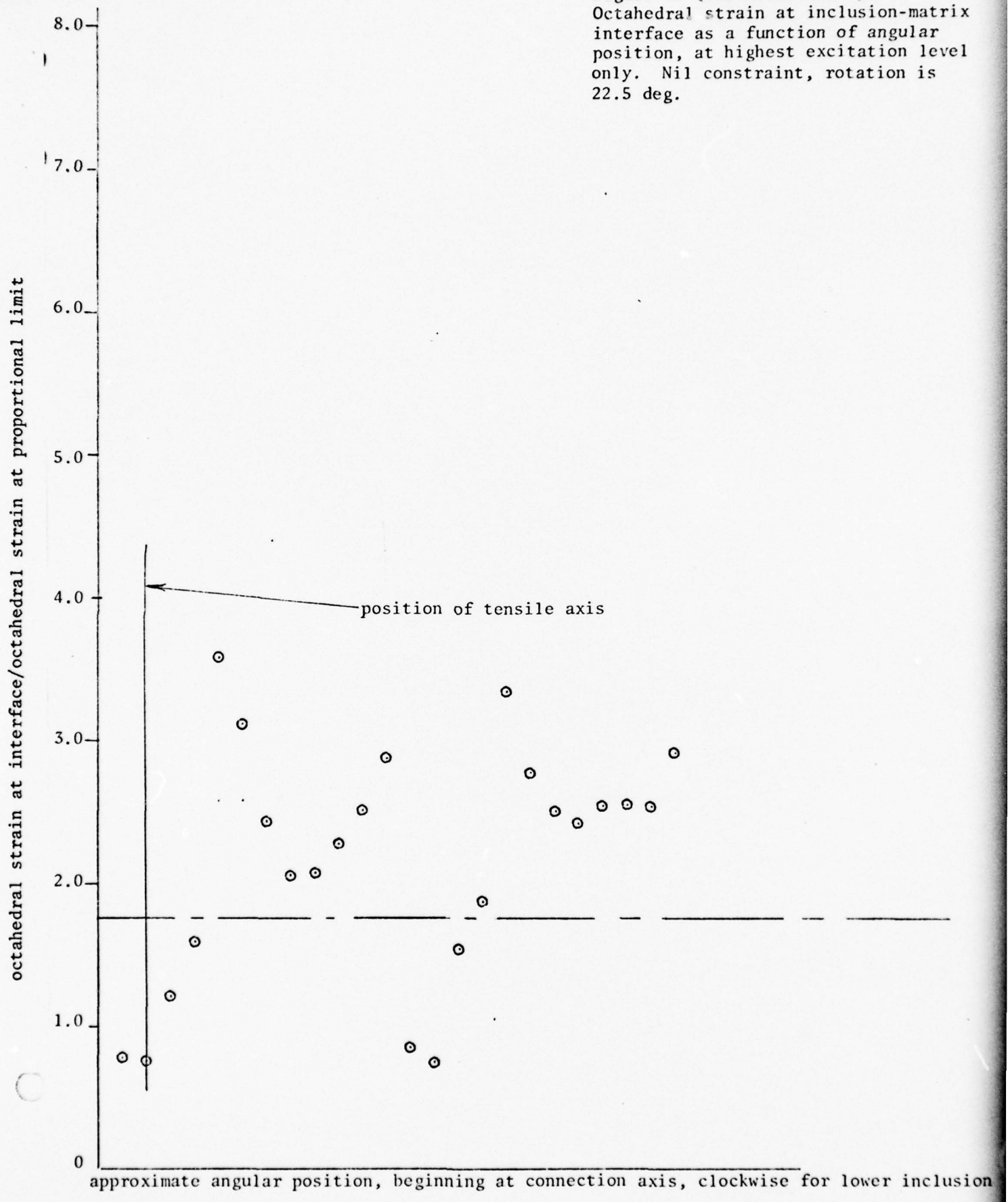

Figure 7c (for burst model): Octahedral strain at inclusion-matrix interface as a function of angular position, at highest excitation level only. Nil constraint, rotation is 45 deg.

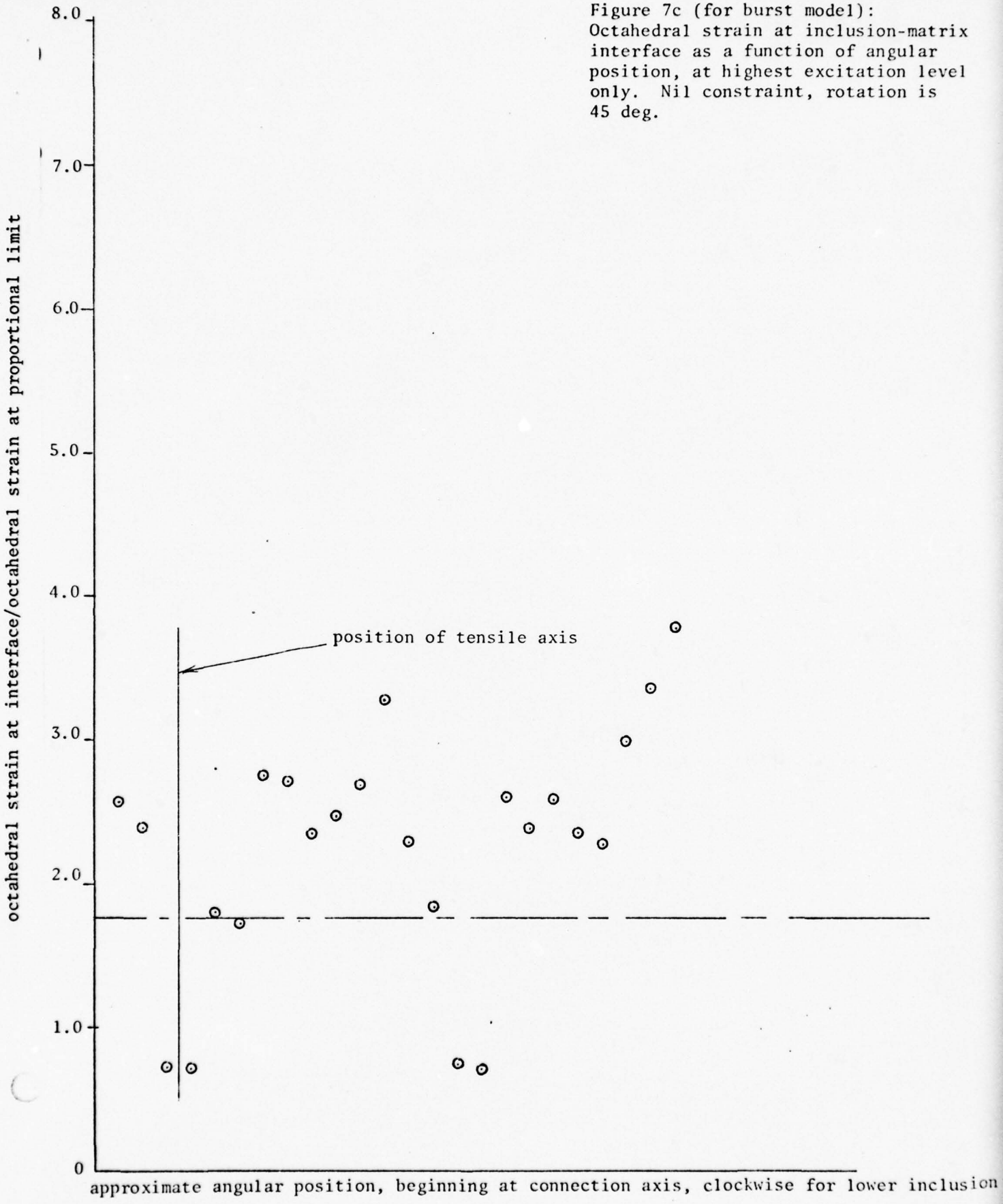

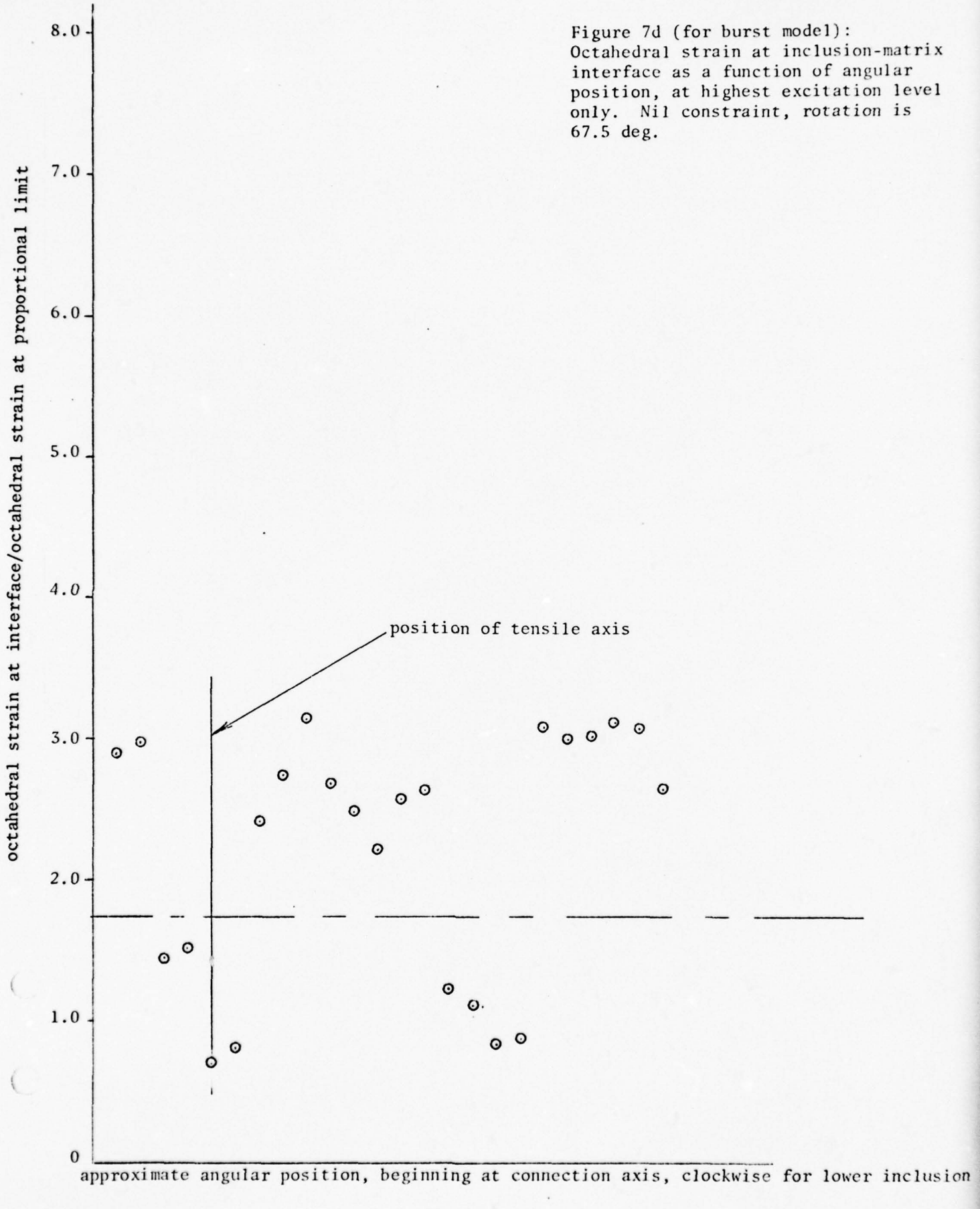

Figure 7d (for burst model): Octahedral strain at inclusion-matrix interface as a function of angular position, at highest excitation level only. Nil constraint, rotation is 67.5 deg.

Figure 7e (for burst model):
Octahedral strain at inclusion-matrix interface as a function of angular position, at highest excitation level only. Nil constraint, rotation is 90 deg.

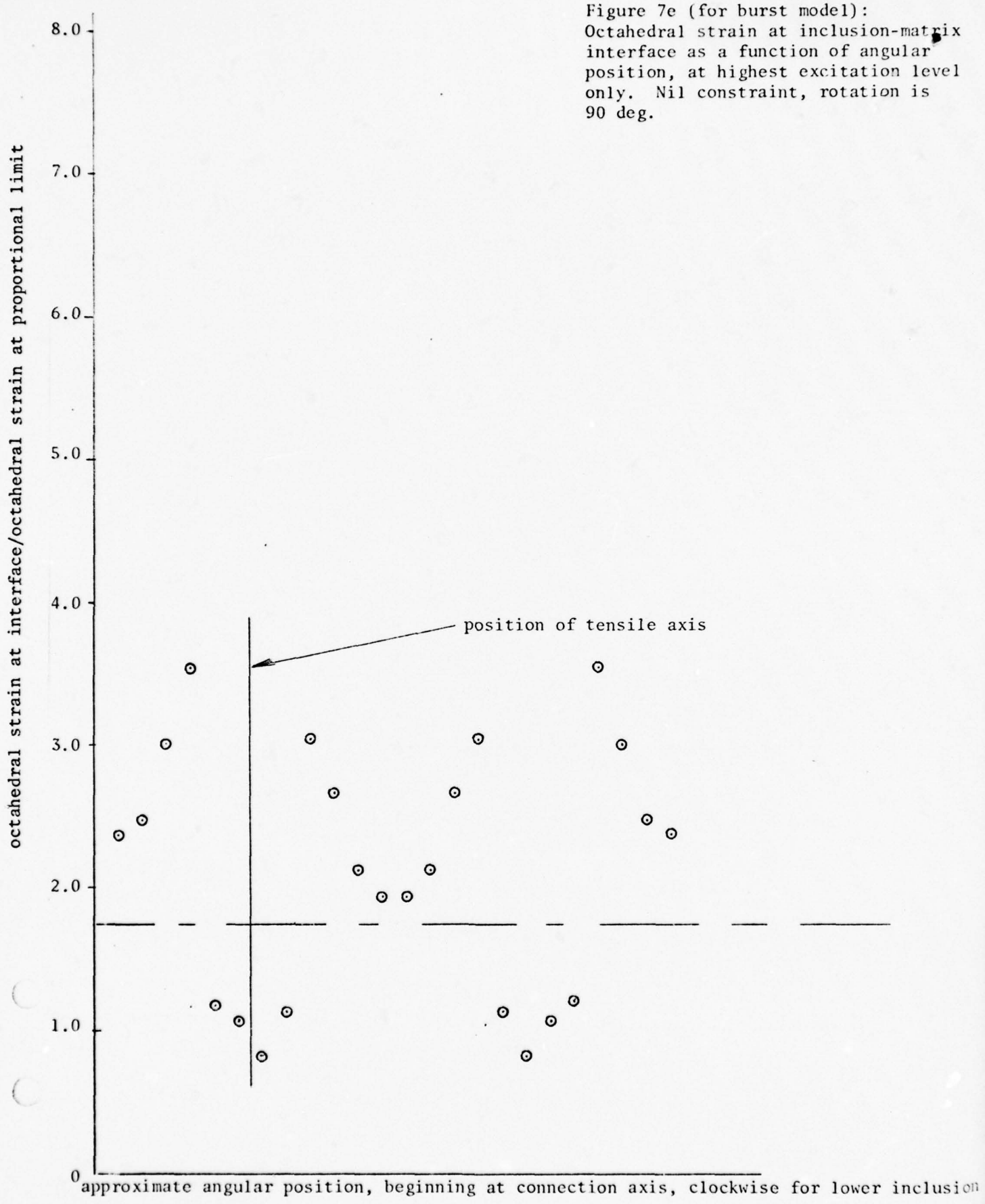

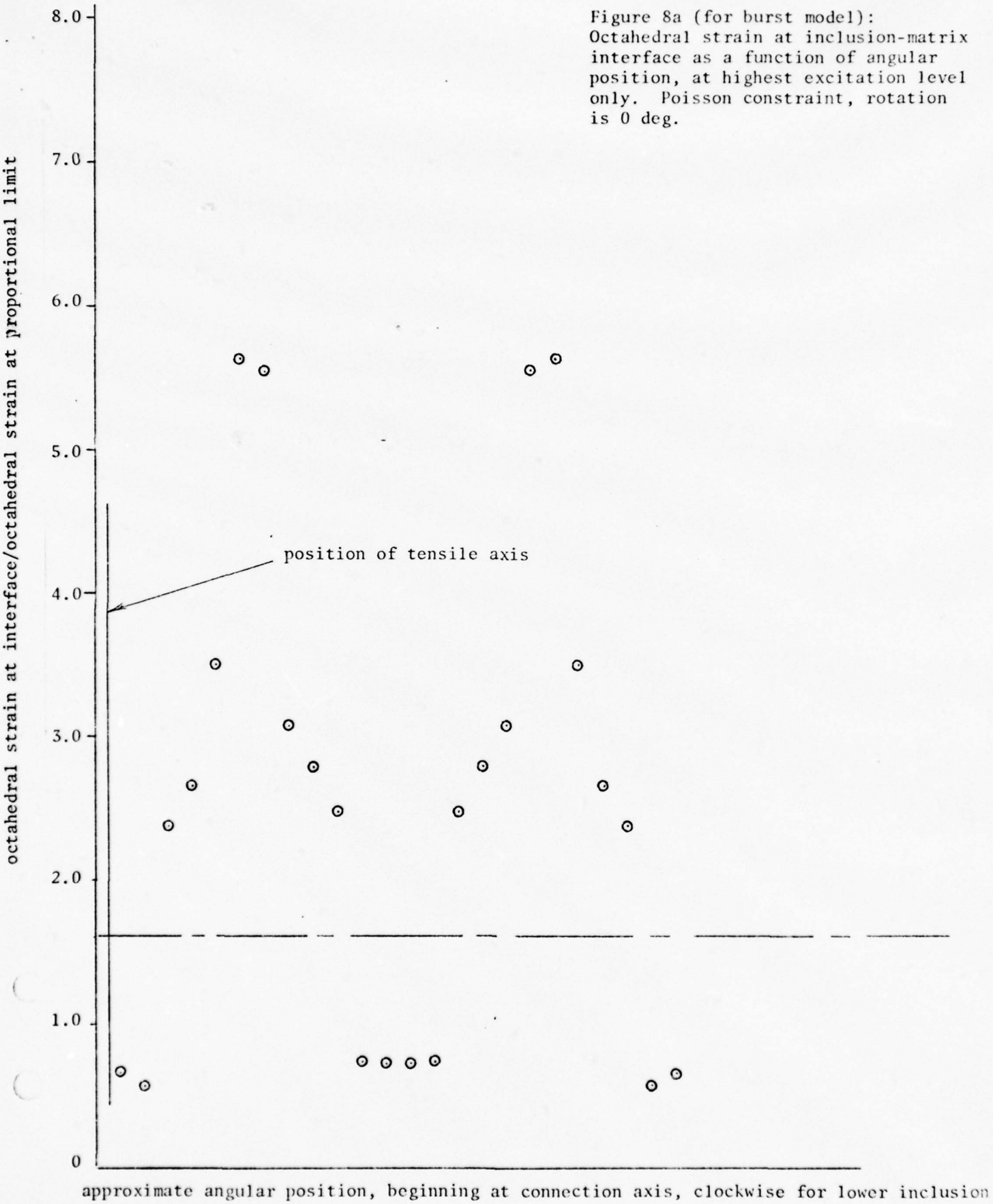

Figure 8a (for burst model): Octahedral strain at inclusion-matrix interface as a function of angular position, at highest excitation level only. Poisson constraint, rotation is 0 deg.

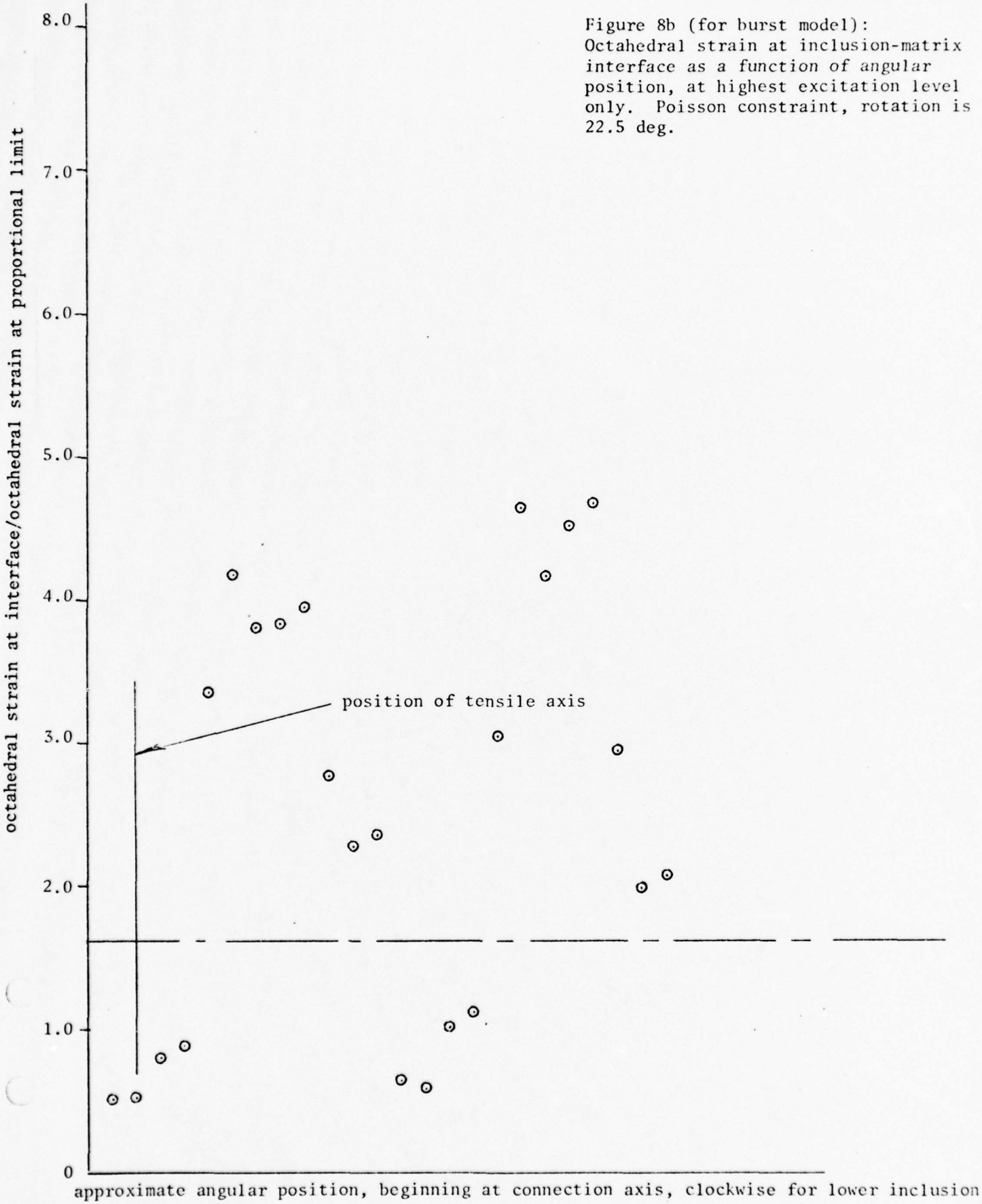

Figure 8b (for burst model): Octahedral strain at inclusion-matrix interface as a function of angular position, at highest excitation level only. Poisson constraint, rotation is 22.5 deg.

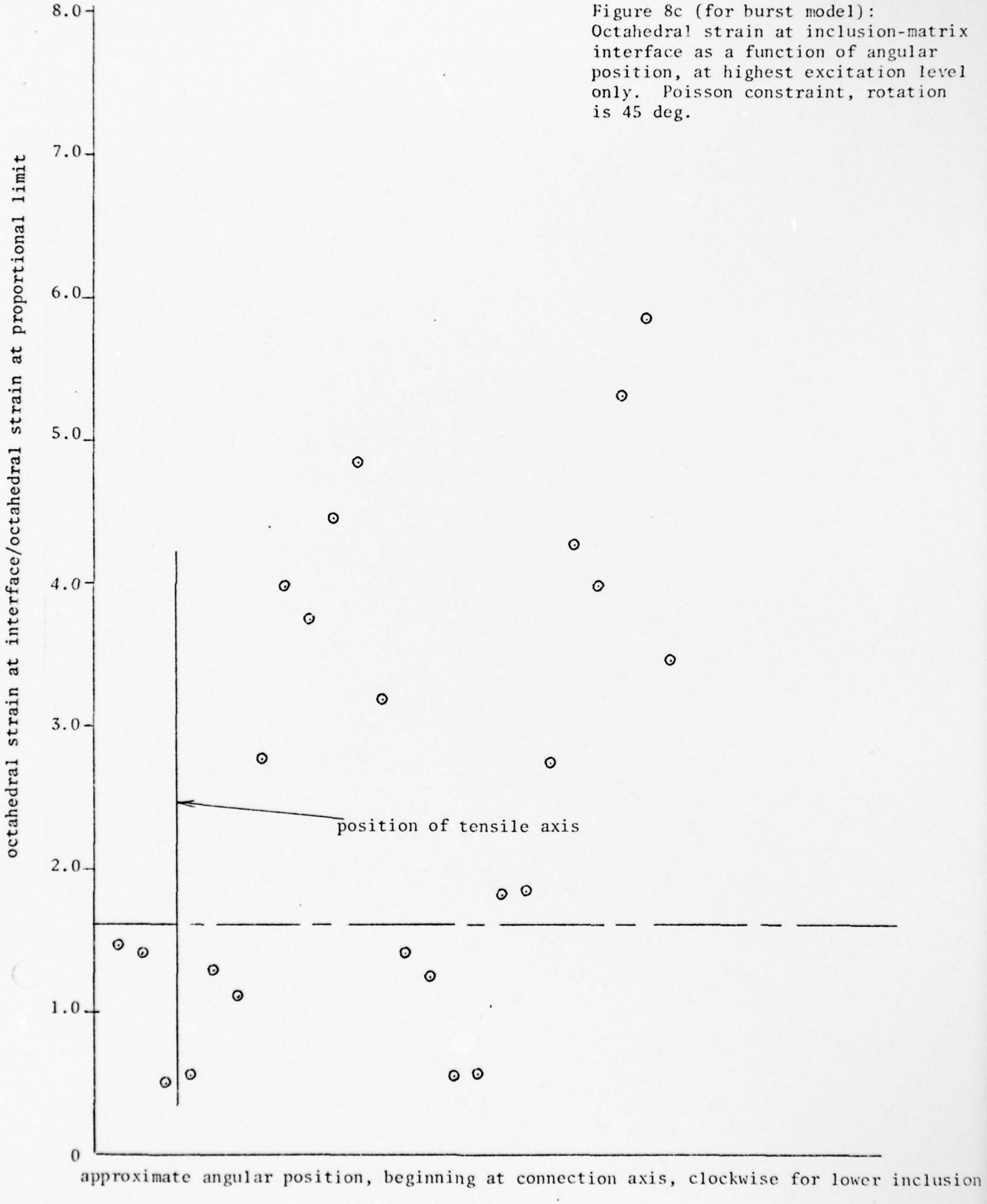

Figure 8c (for burst model): Octahedral strain at inclusion-matrix interface as a function of angular position, at highest excitation level only. Poisson constraint, rotation is 45 deg.

Figure 8d (for burst model):
Octahedral strain at inclusion-matrix interface as a function of angular position, at highest excitation level only. Poisson constraint, rotation is 67.5 deg.

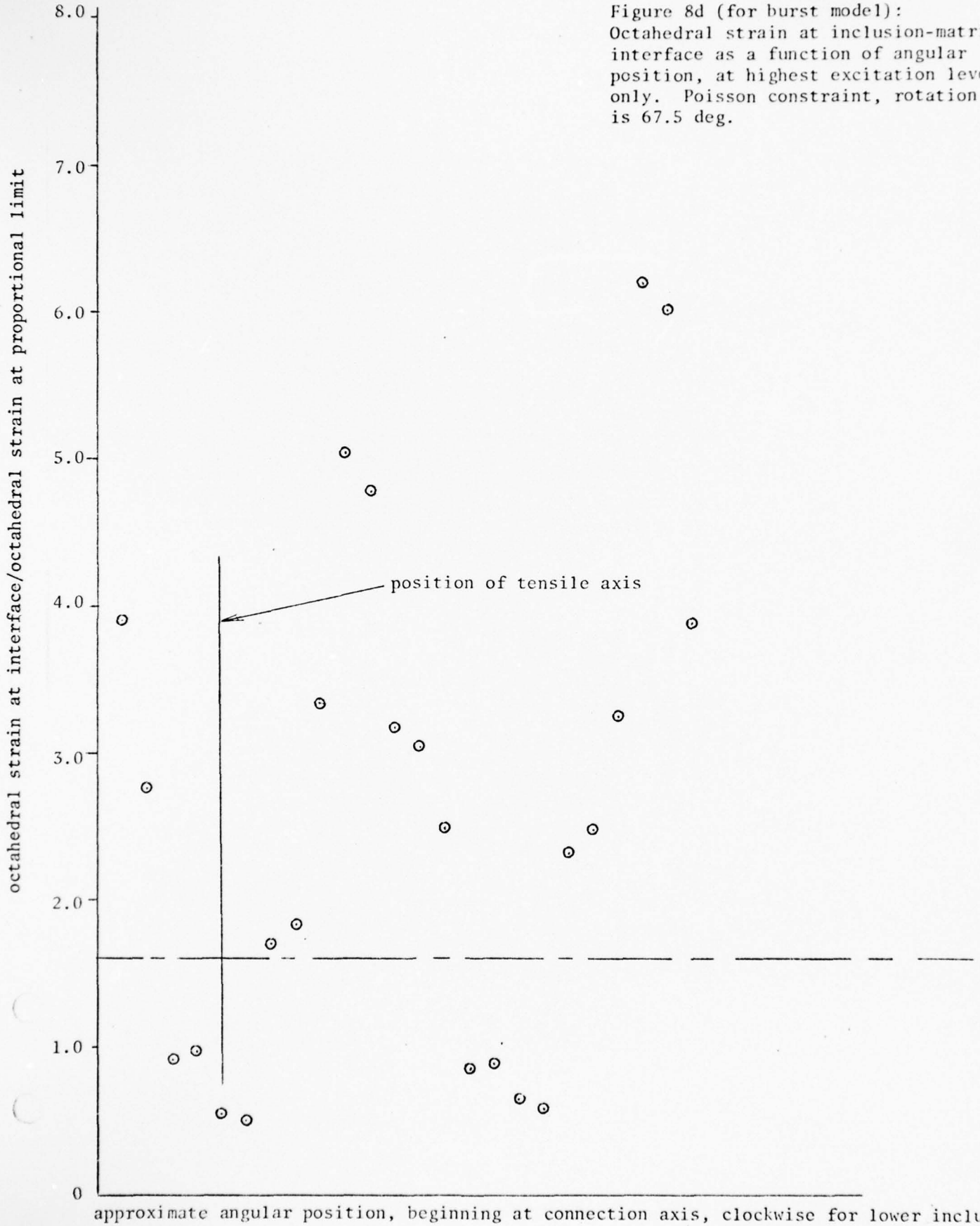

Figure 8e (for burst model)
Octahedral strain at inclusion-matrix interface as a function of angular position, at highest excitation level only. Poisson constraint, rotation is 90 deg.

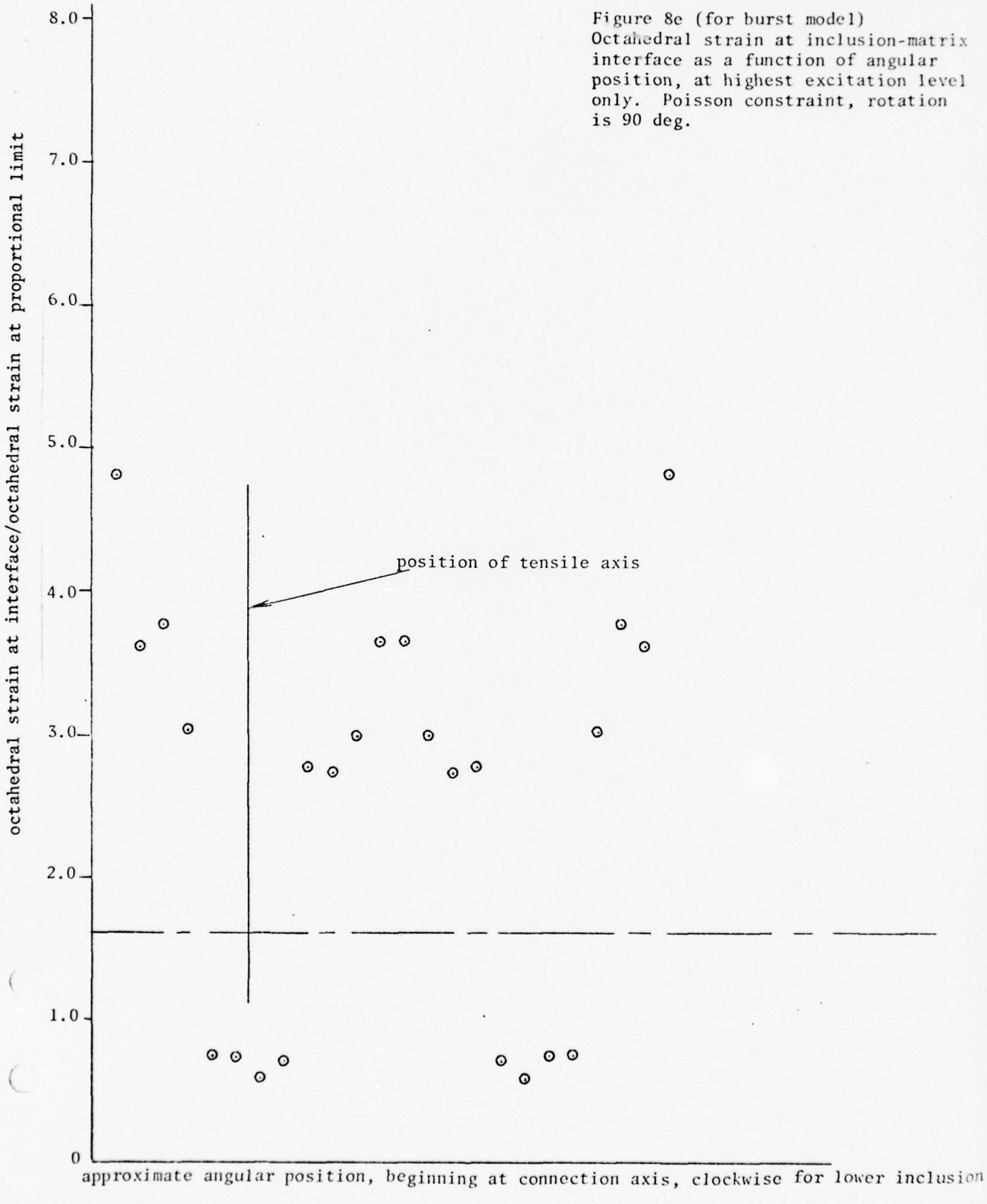

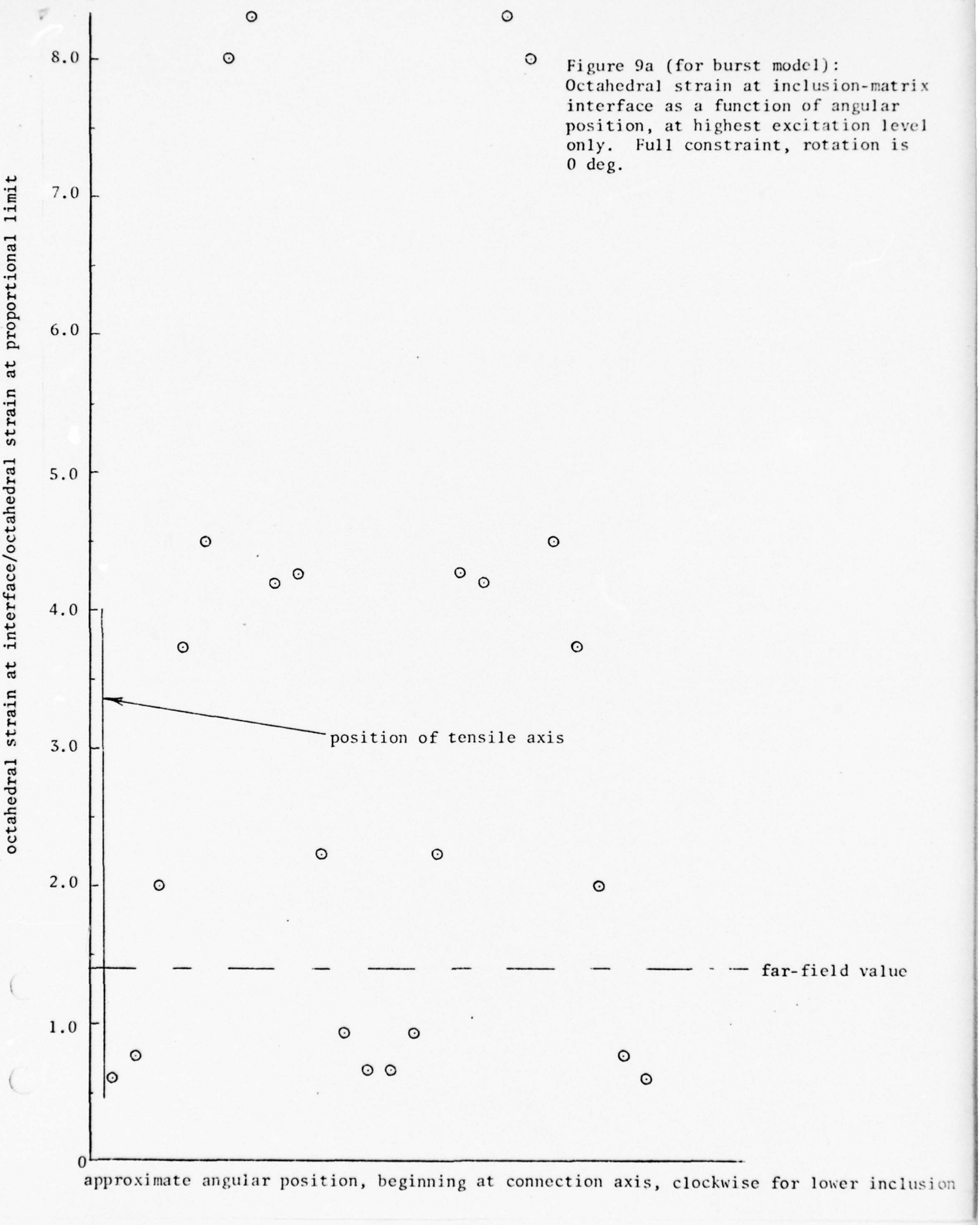

Figure 9a (for burst model): Octahedral strain at inclusion-matrix interface as a function of angular position, at highest excitation level only. Full constraint, rotation is 0 deg.

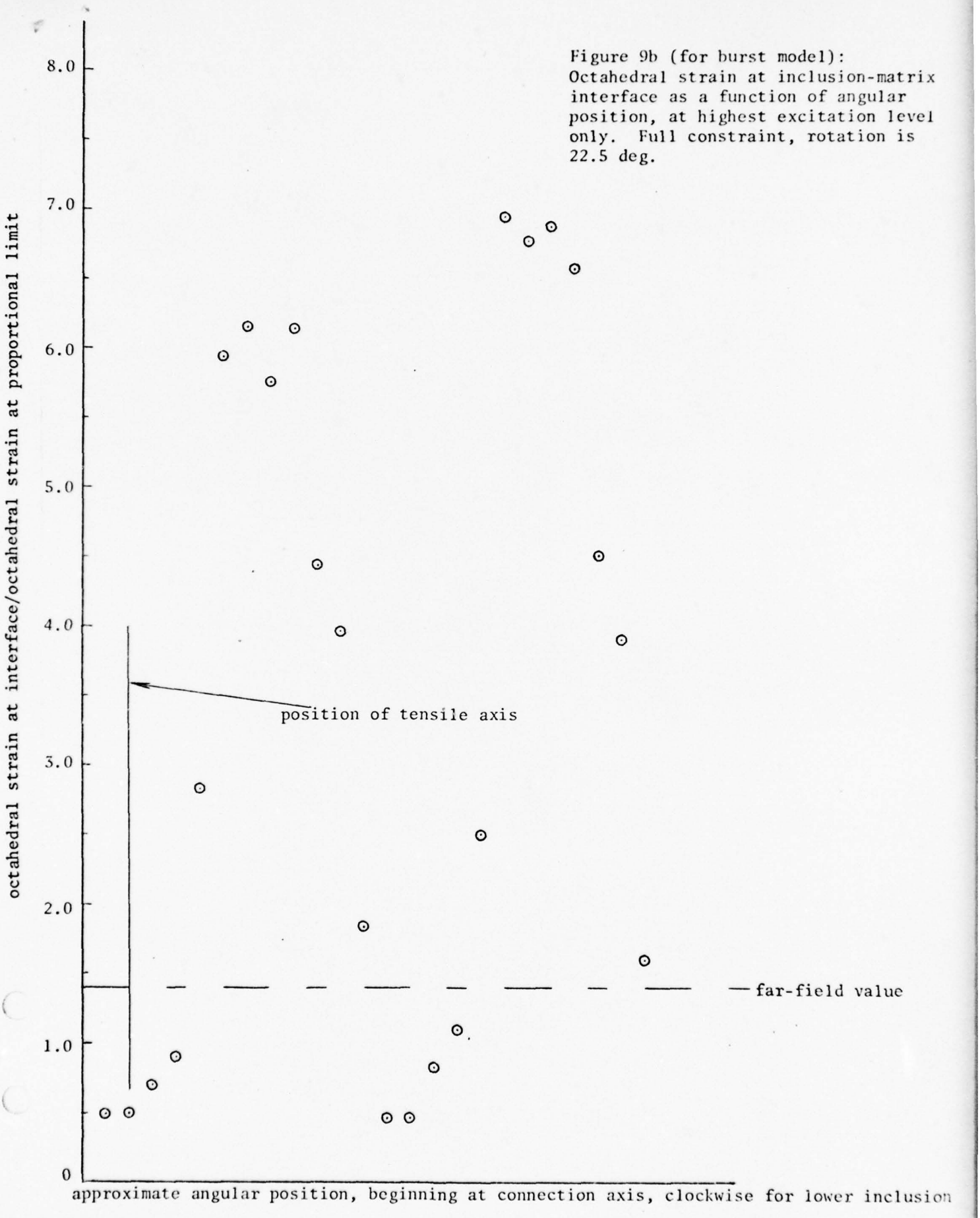

Figure 9b (for burst model): Octahedral strain at inclusion-matrix interface as a function of angular position, at highest excitation level only. Full constraint, rotation is 22.5 deg.

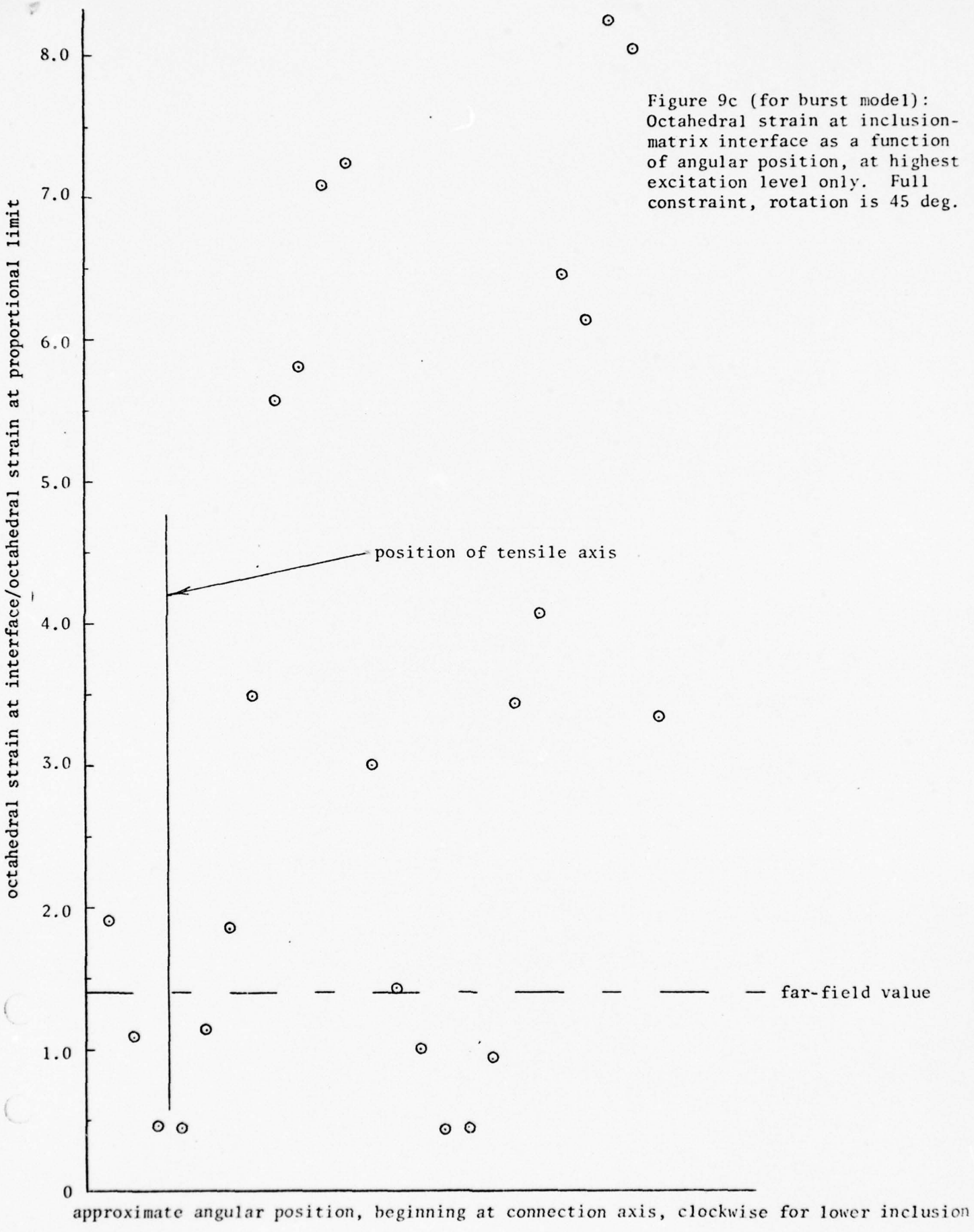

Figure 9c (for burst model): Octahedral strain at inclusion-matrix interface as a function of angular position, at highest excitation level only. Full constraint, rotation is 45 deg.

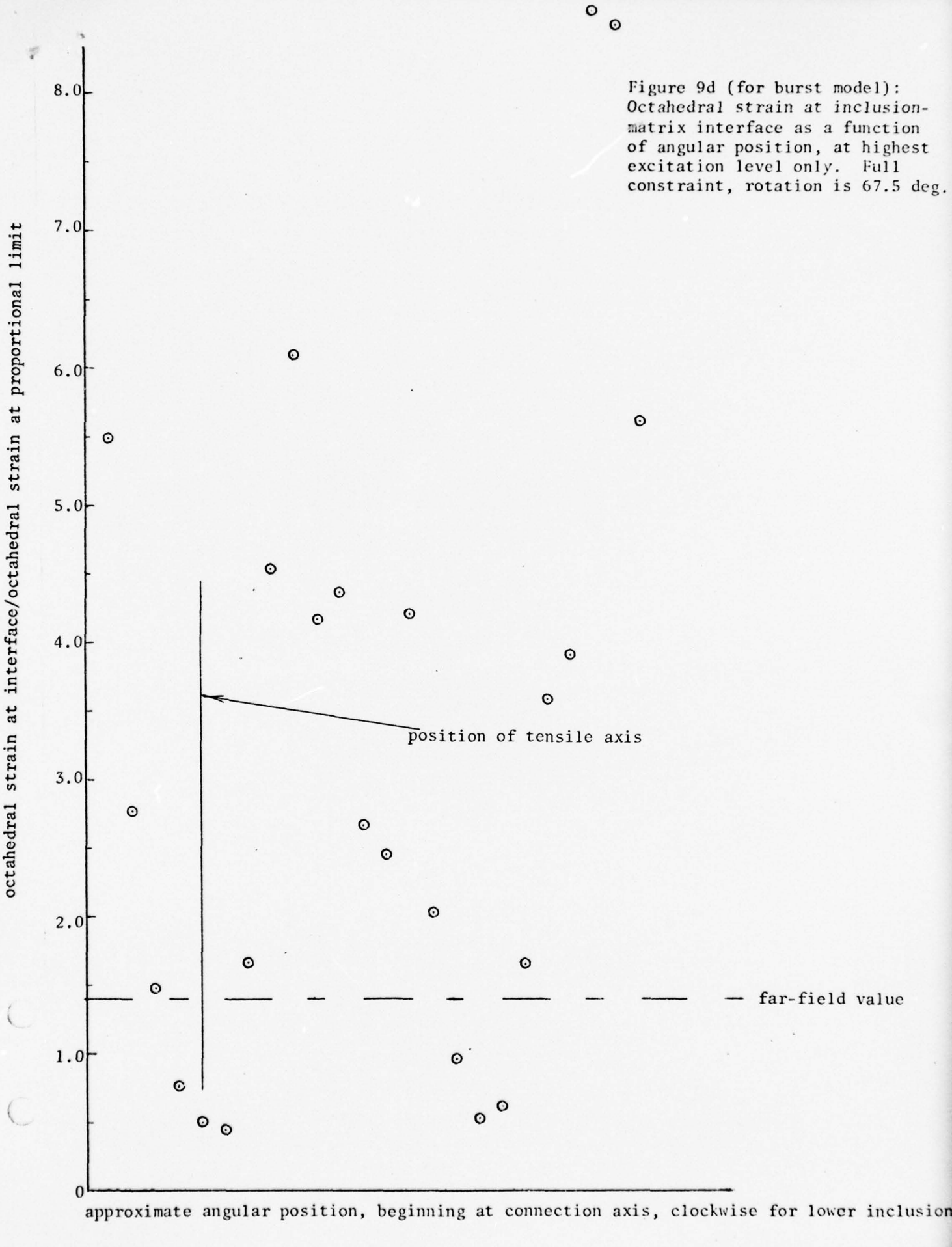

Figure 9d (for burst model): Octahedral strain at inclusion-matrix interface as a function of angular position, at highest excitation level only. Full constraint, rotation is 67.5 deg.

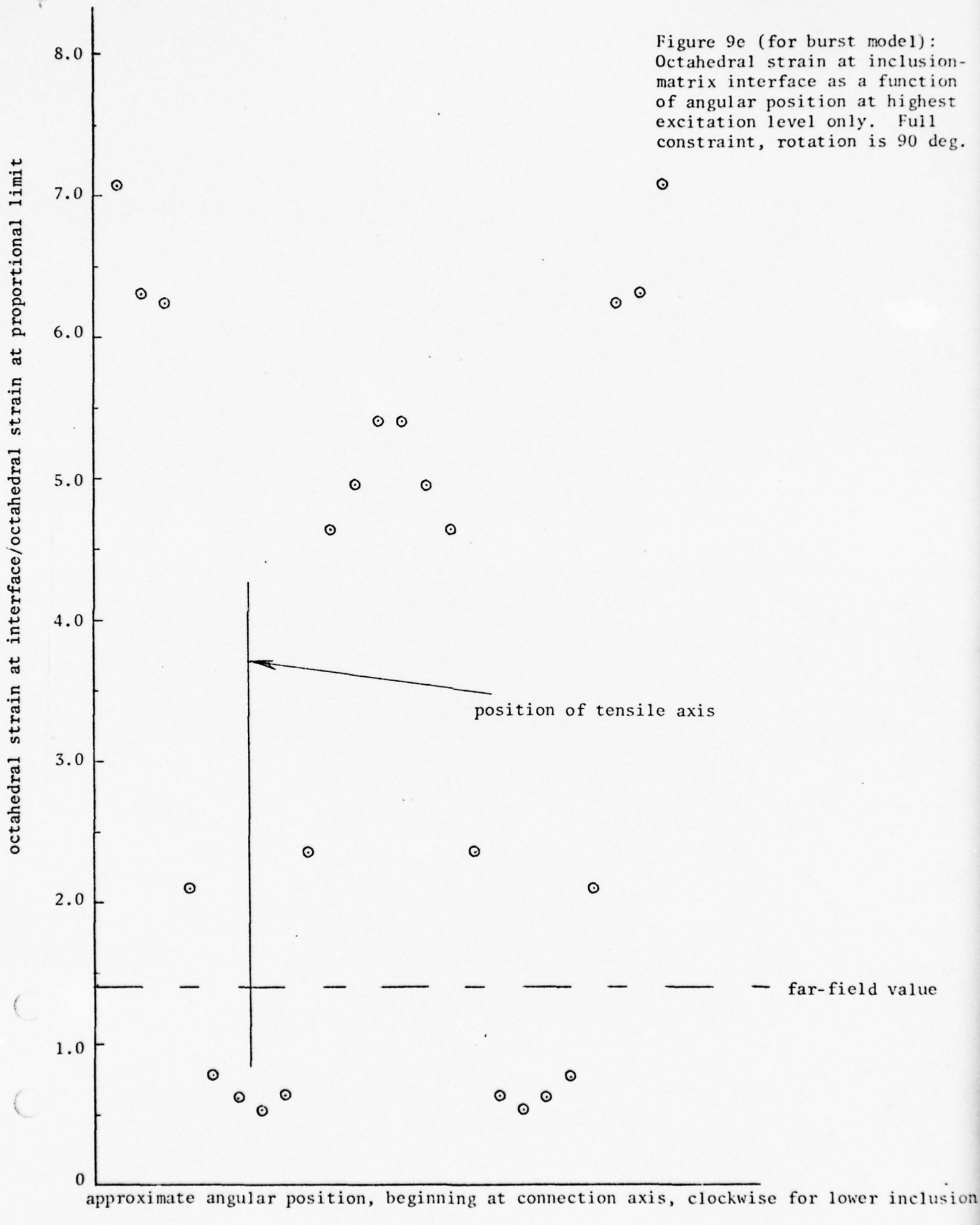

Figure 9e (for burst model): Octahedral strain at inclusion-matrix interface as a function of angular position at highest excitation level only. Full constraint, rotation is 90 deg.

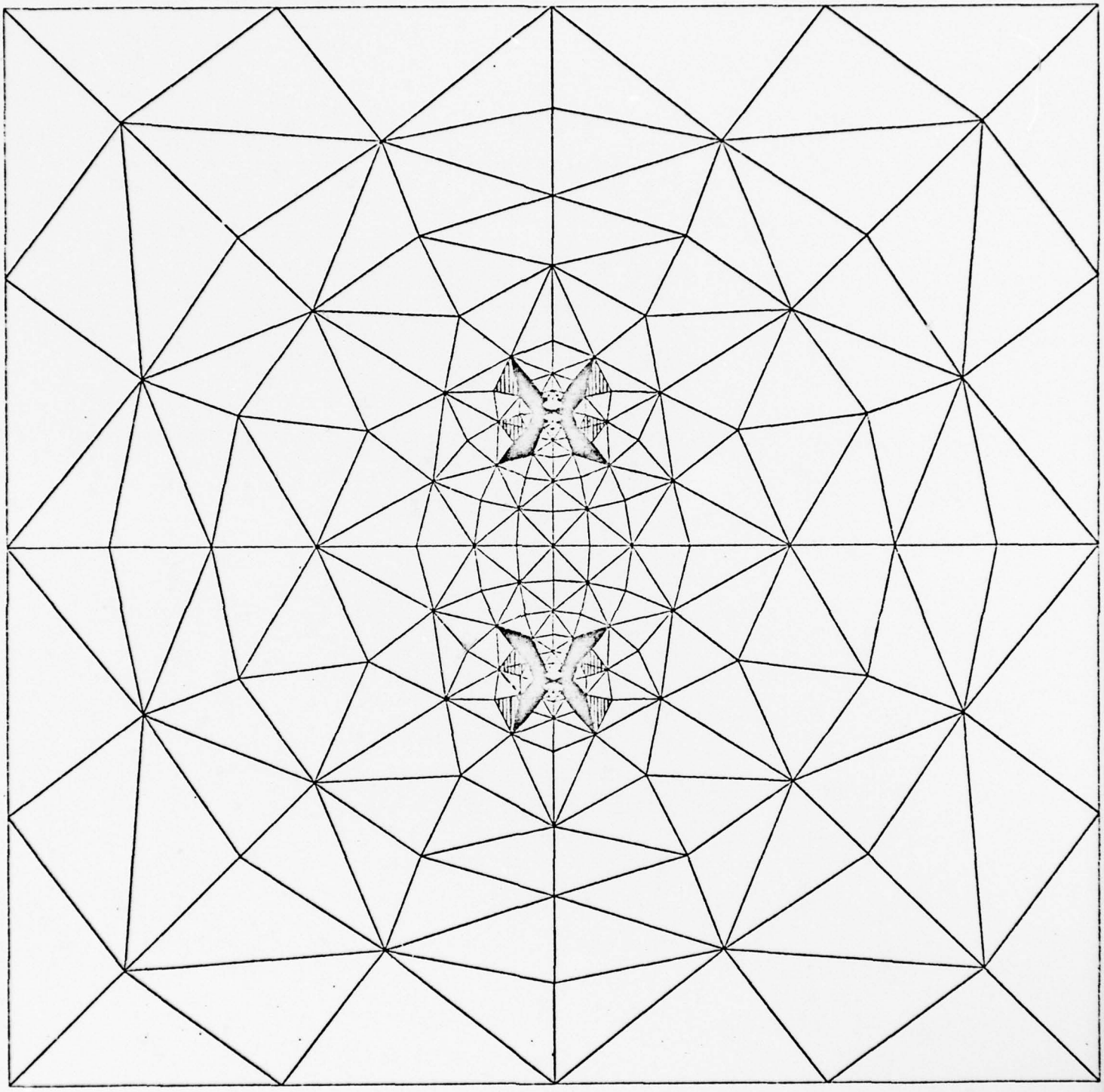

Figure 10a. Cross-hatched area shows octahedral strain exceeding far-field value by 5 percent, and solid area by 10 percent; nil constraint, rotation is 0 deg, burst model

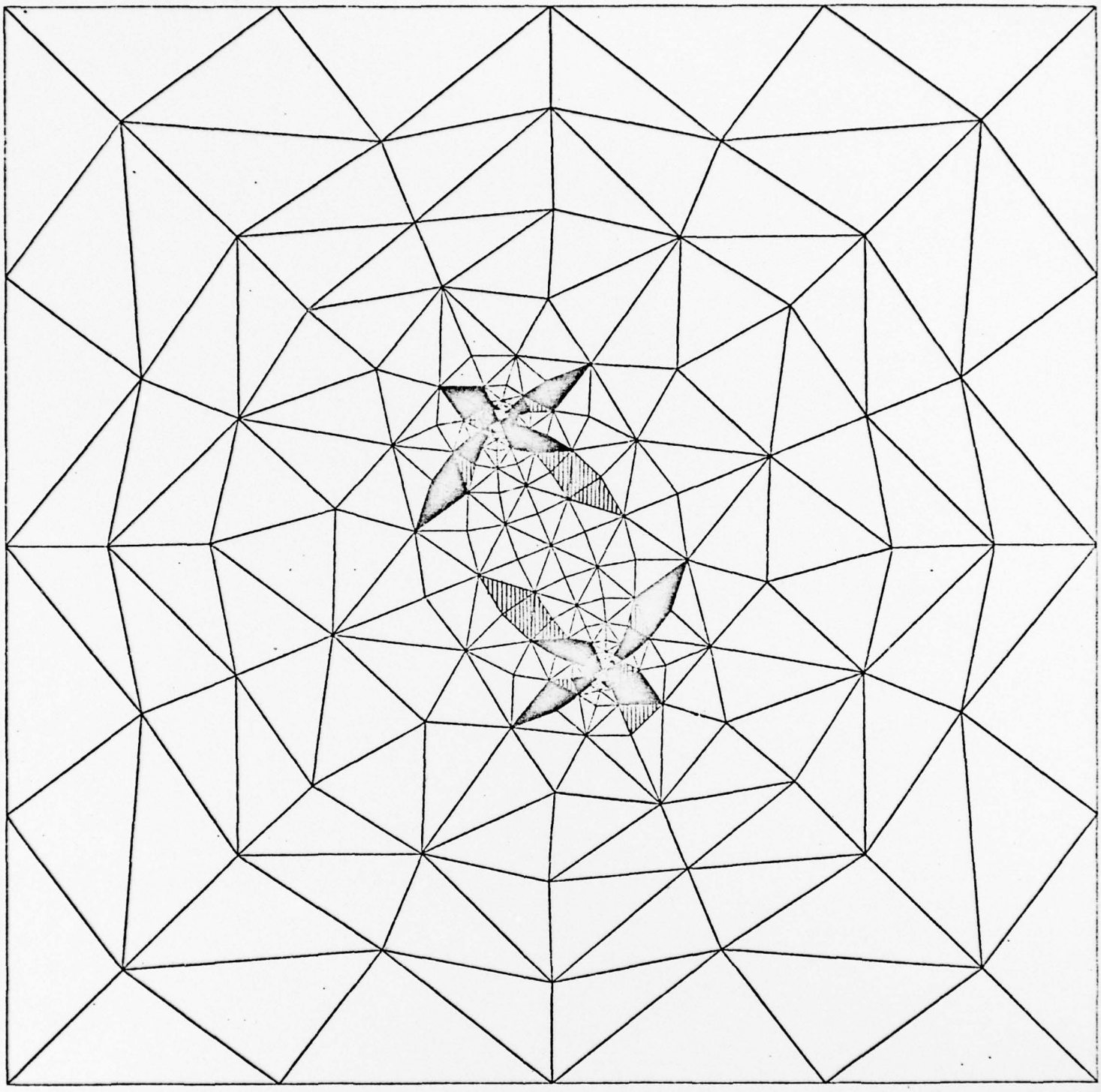

Figure 10b. Cross-hatched area shows octahedral strain exceeding far-field value by 5 percent, and solid area by 10 percent; nil constraint, rotation is 22.5 deg, burst model

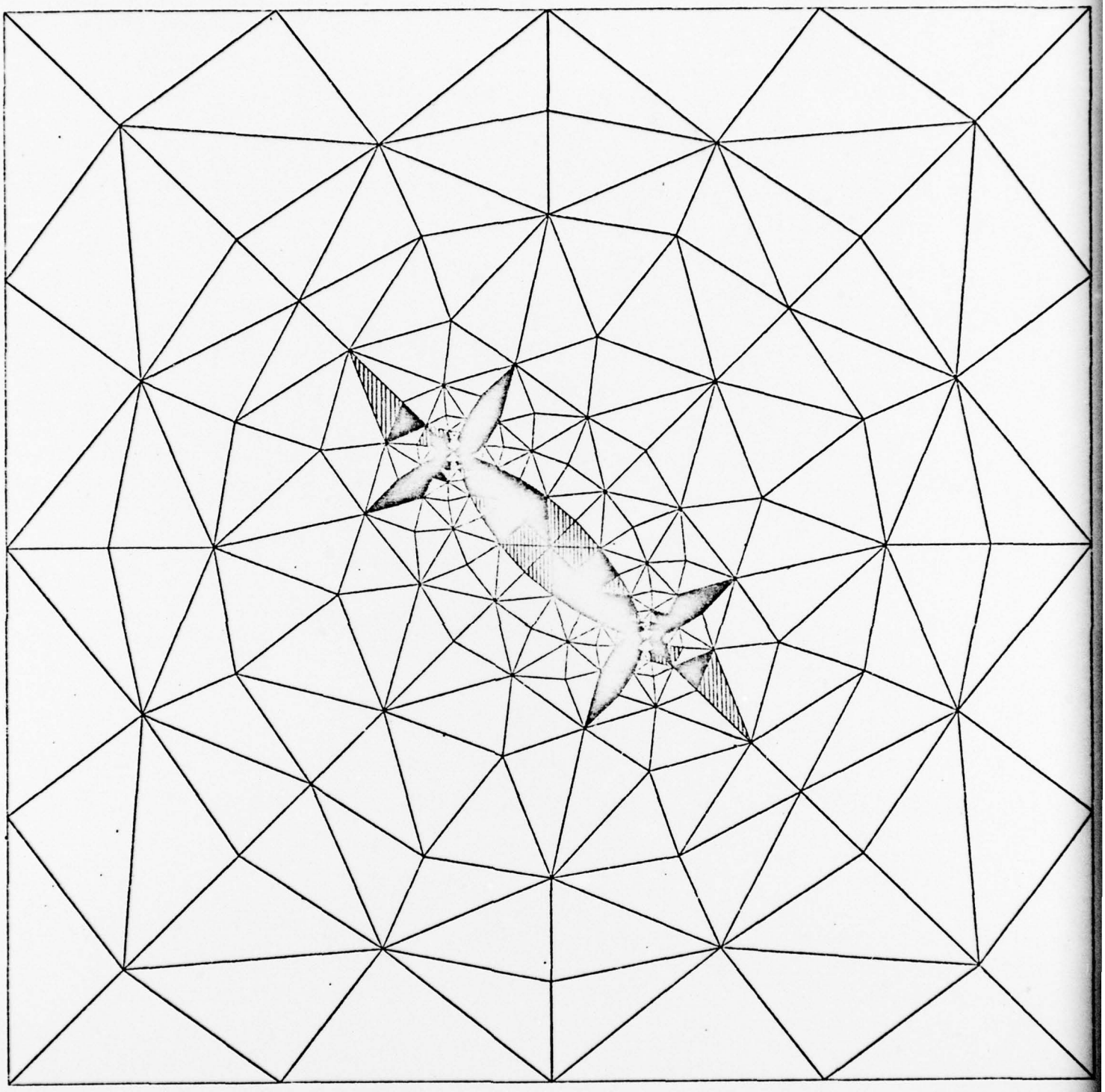

Figure 10c. Cross-hatched area shows octahedral strain exceeding far-field value by 5 percent, and solid area by 10 percent; nil constraint, rotation is 45 deg, burst model

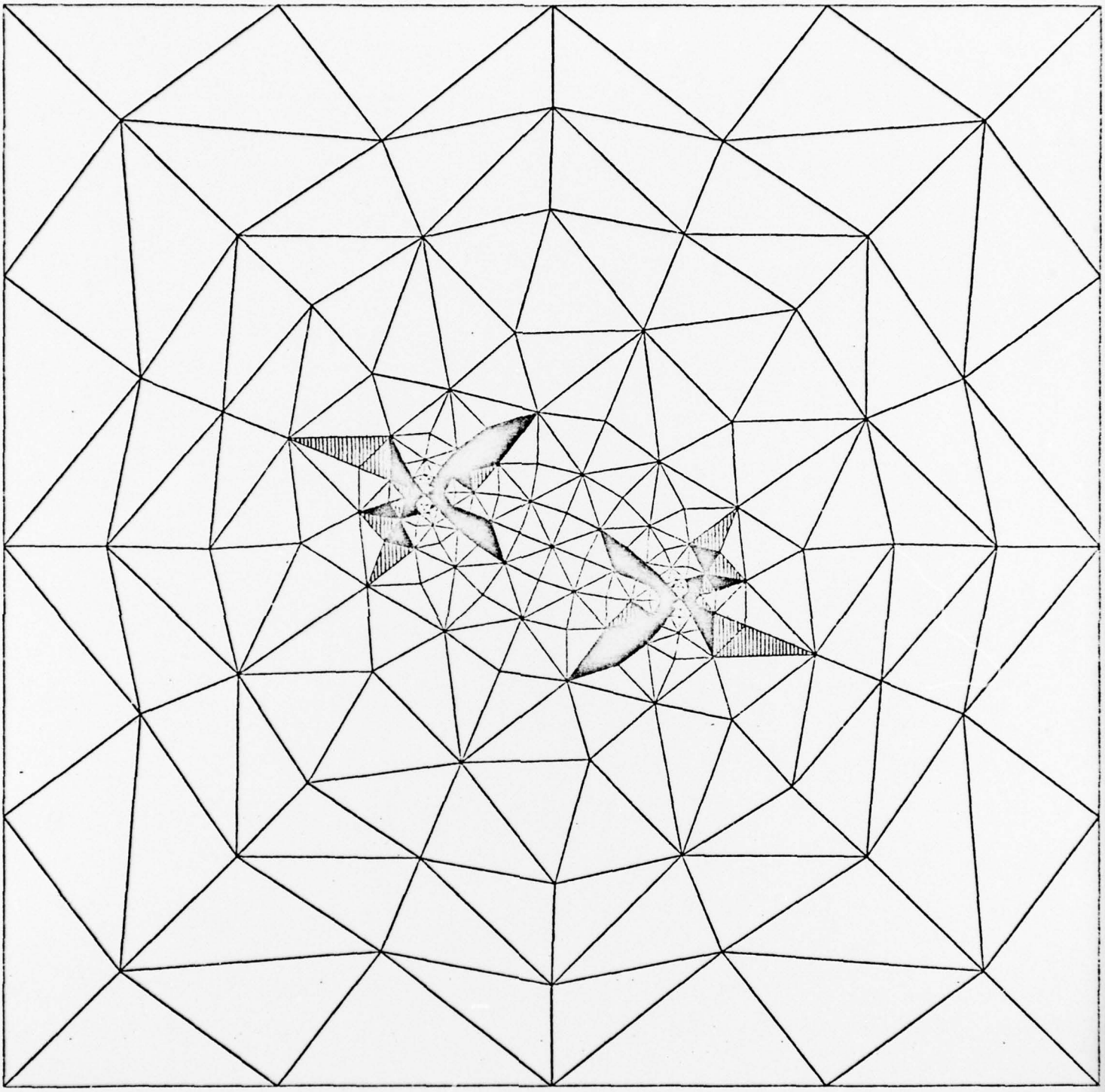

Figure 10d. Cross-hatched area shows octahedral strain exceeding far-field value by 5 percent, and solid area by 10 percent; nil constraint, rotation is 67.5 deg, burst model

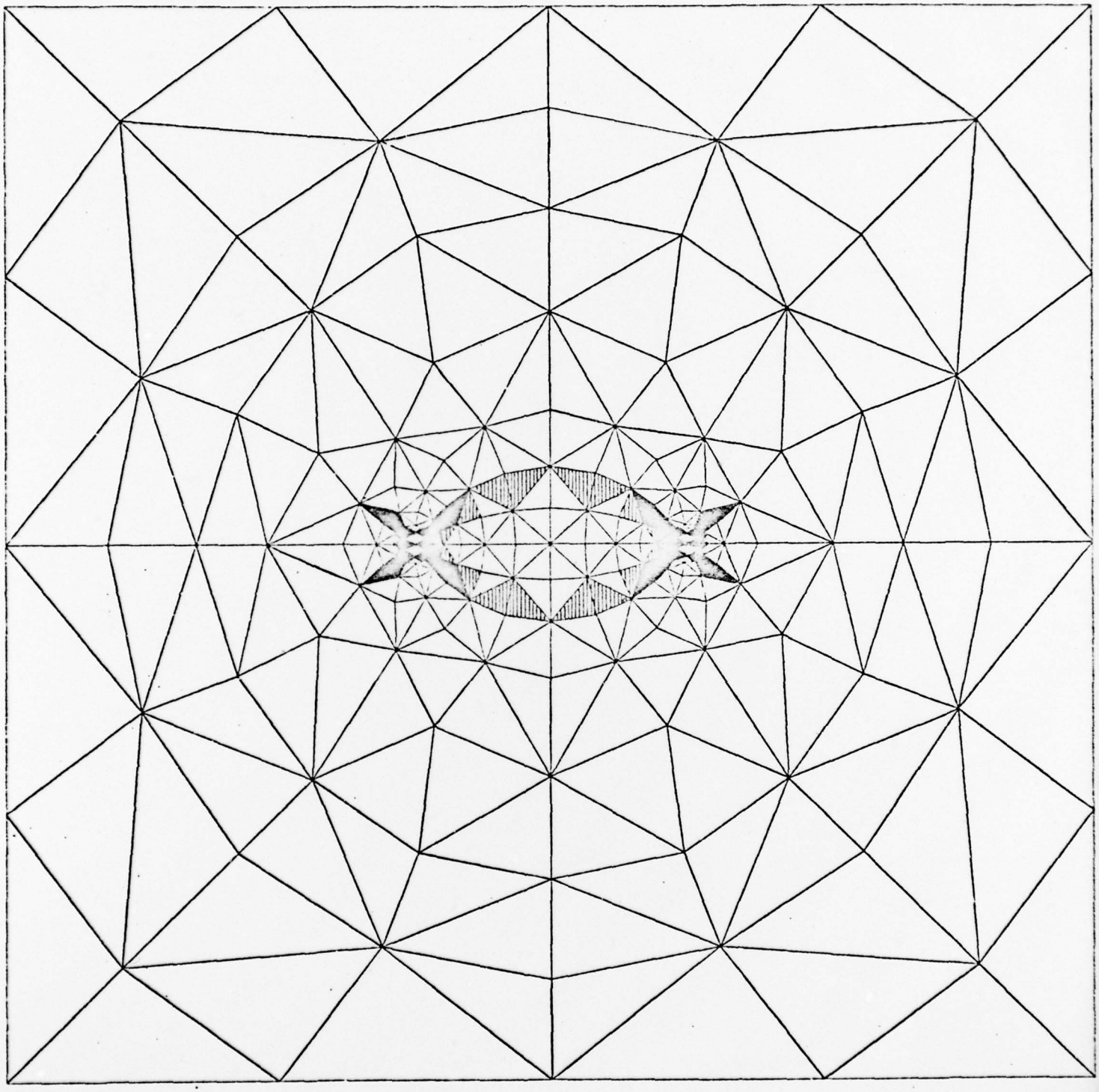

Figure 10e. Cross-hatched area shows octahedral strain exceeding far-field value by 5 percent, and solid area by 10 percent; nil constraint, rotation is 90 deg, burst model

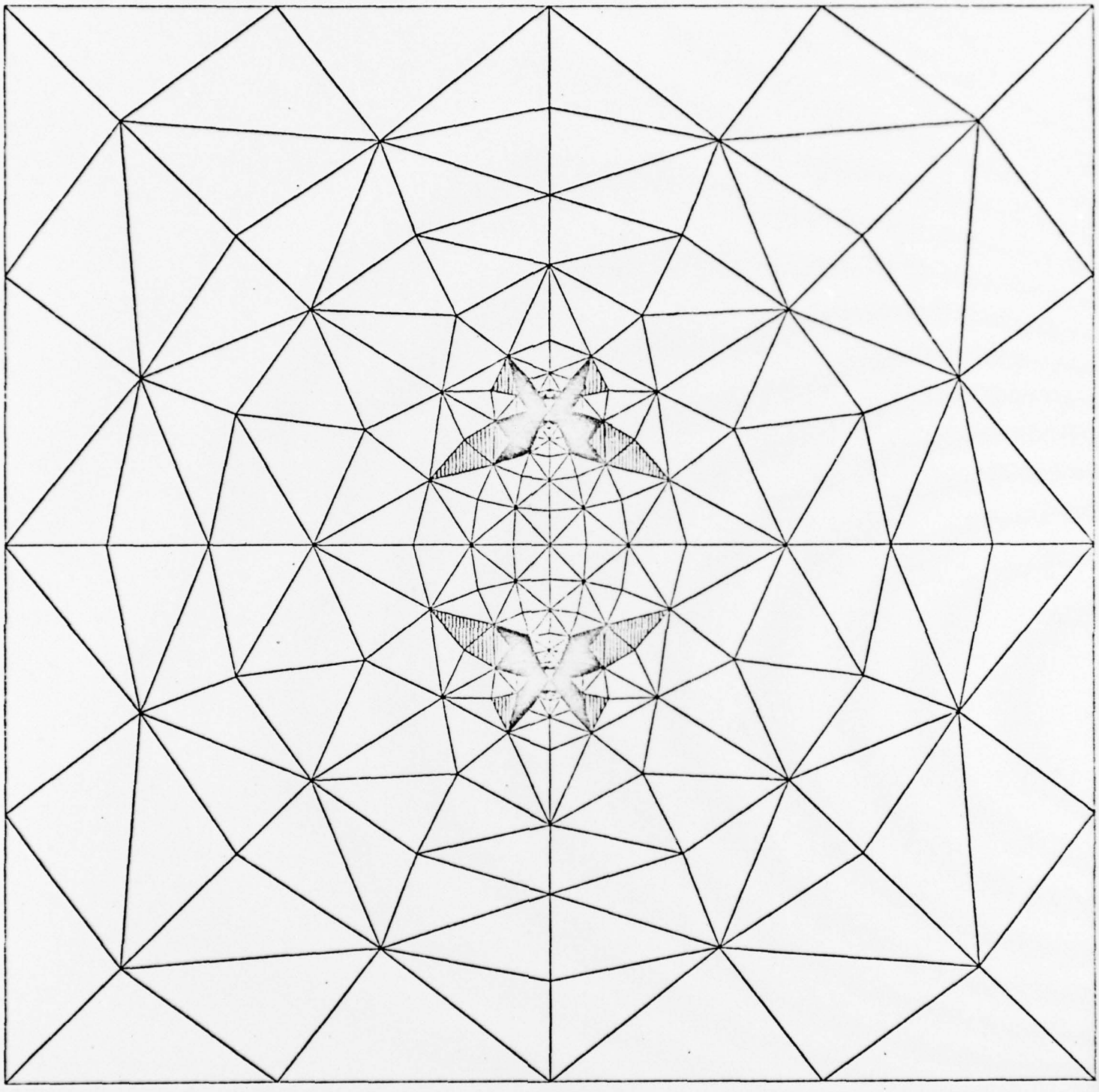

Figure 11a. Cross-hatched area shows octahedral strain exceeding far-field value by 5 percent, and solid area by 10 percent; Poisson constraint, rotation is 0 deg, burst model

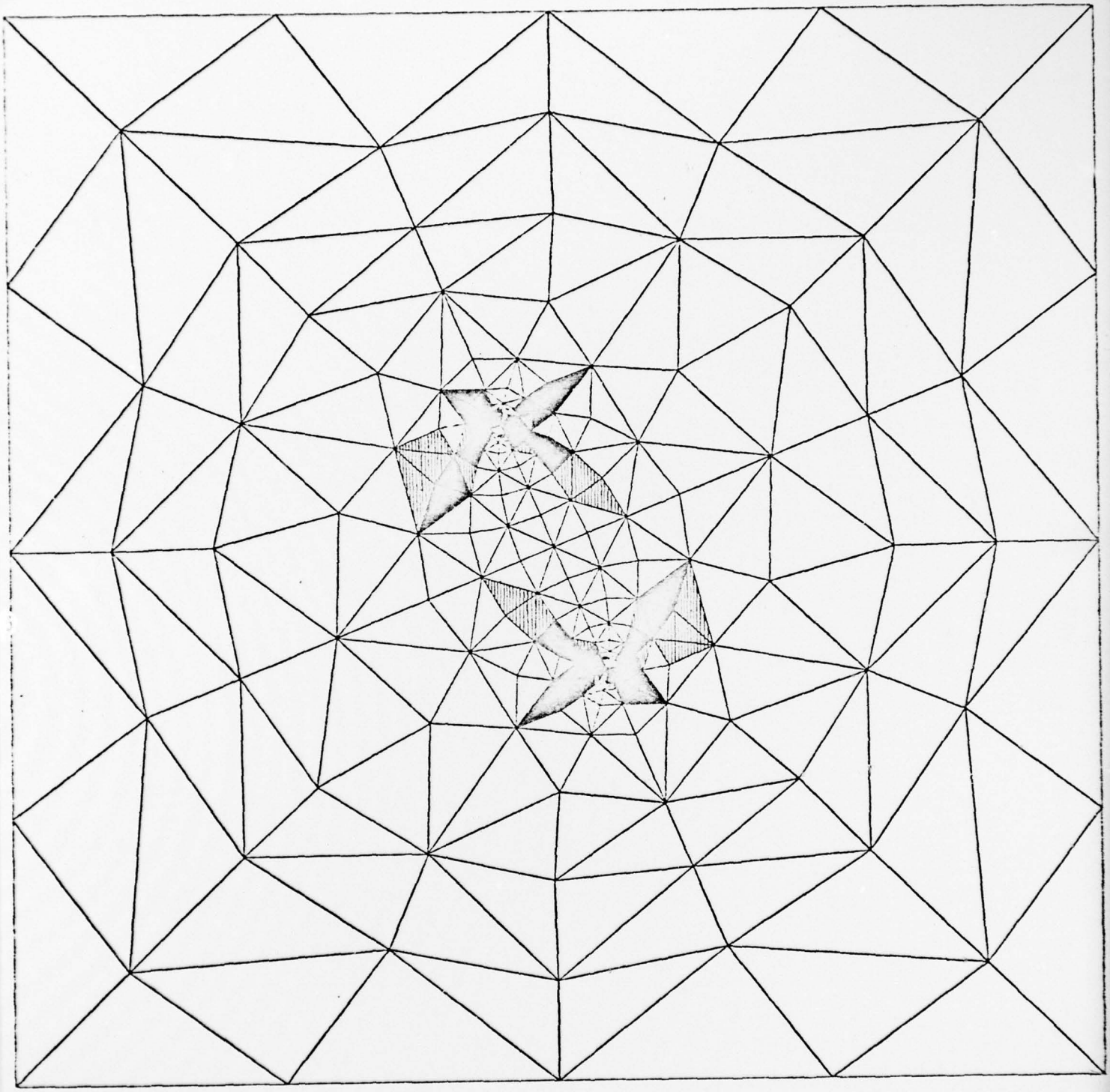

Figure 11b. Cross-hatched area shows octahedral strain exceeding far-field value by 5 percent, and solid area by 10 percent; Poisson constraint, rotation is 22.5 deg, burst model

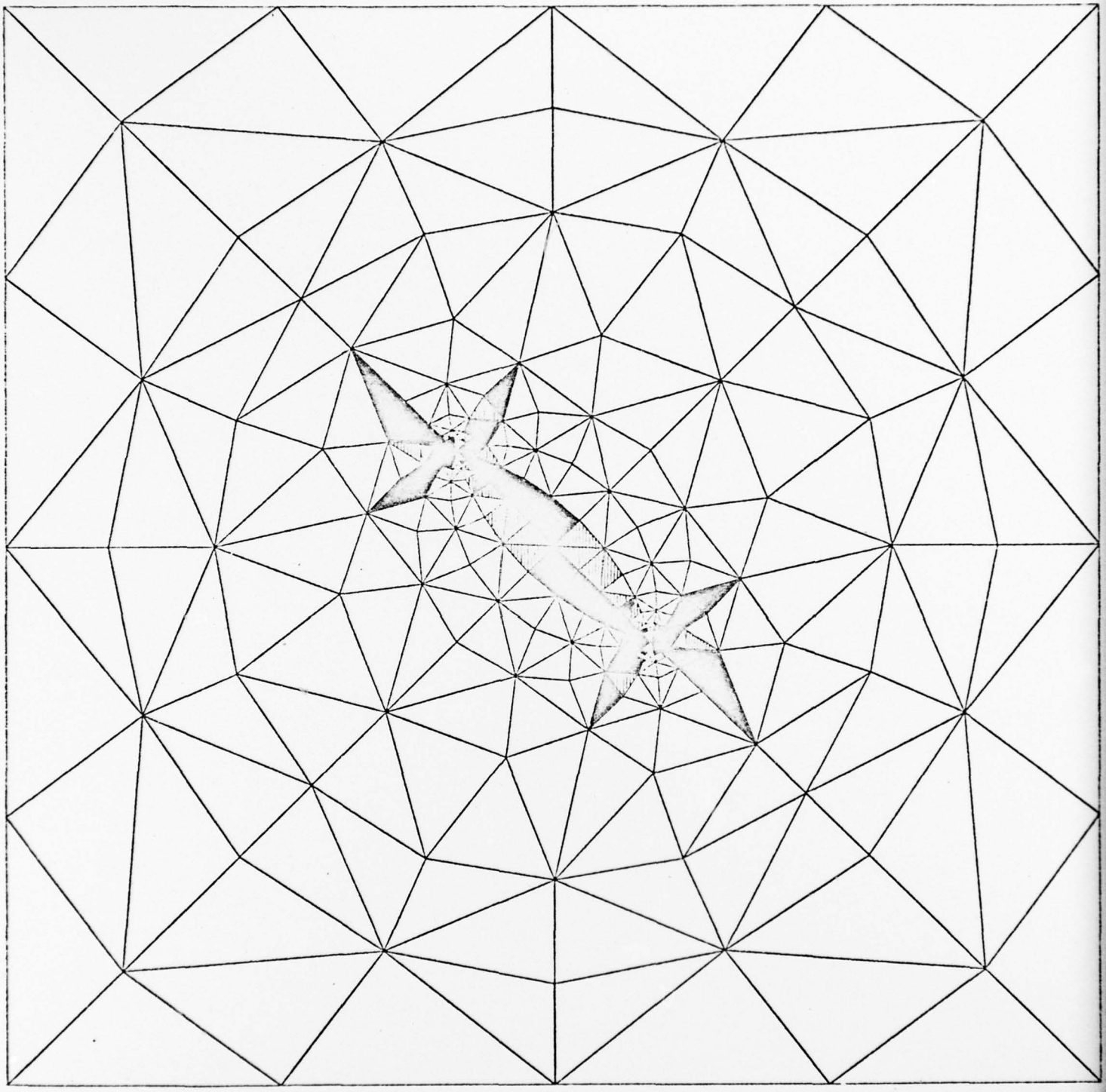

Figure 11c. Cross-hatched area shows octahedral strain exceeding far-field value by 5 percent, and solid area by 10 percent; Poisson constraint, rotation is 45 deg, burst model

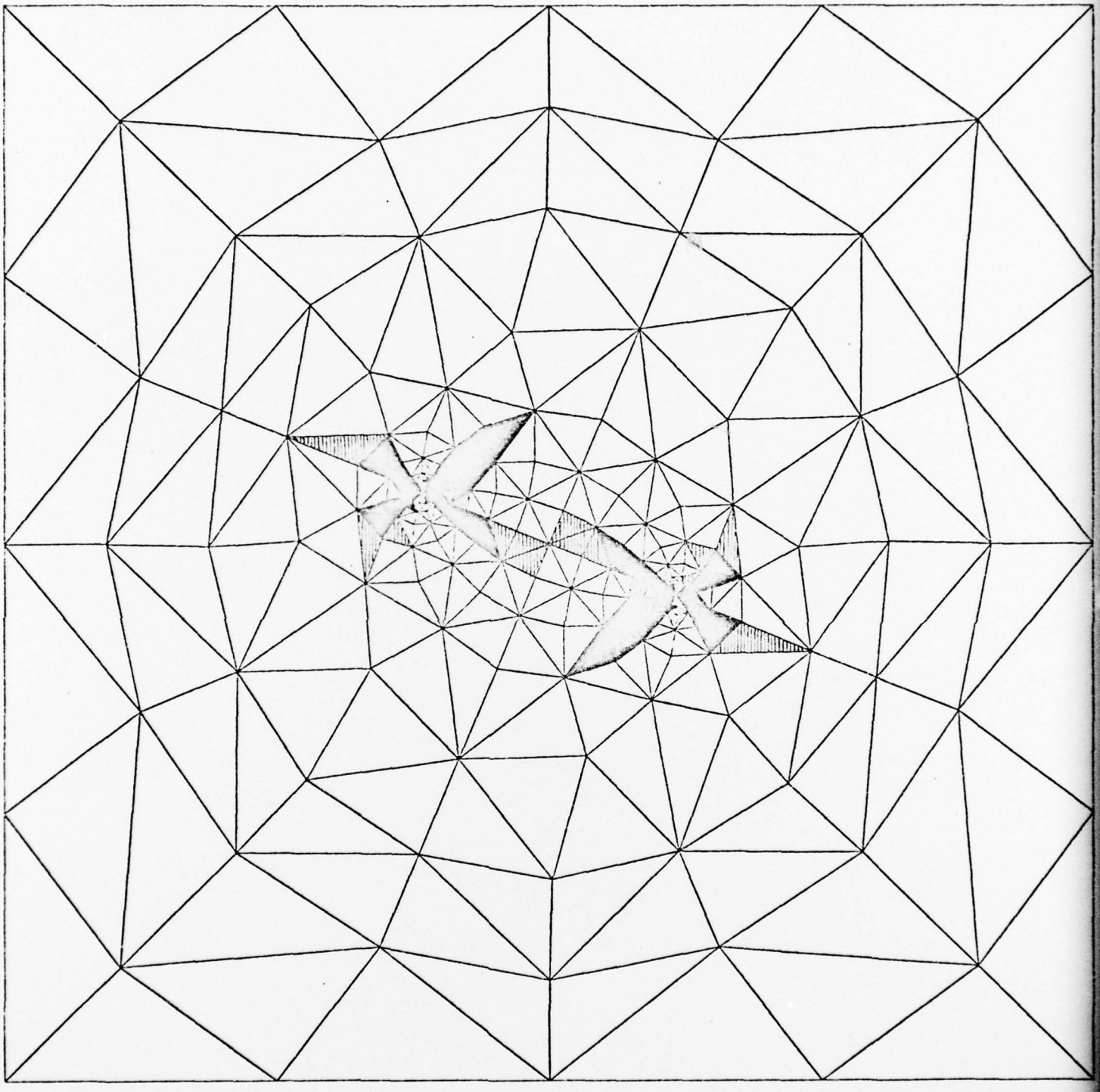

Figure 11d. Cross-hatched area shows octahedral strain exceeding far-field value by 5 percent, and solid area by 10 percent; Poisson constraint, rotation is 67.5 deg, burst model

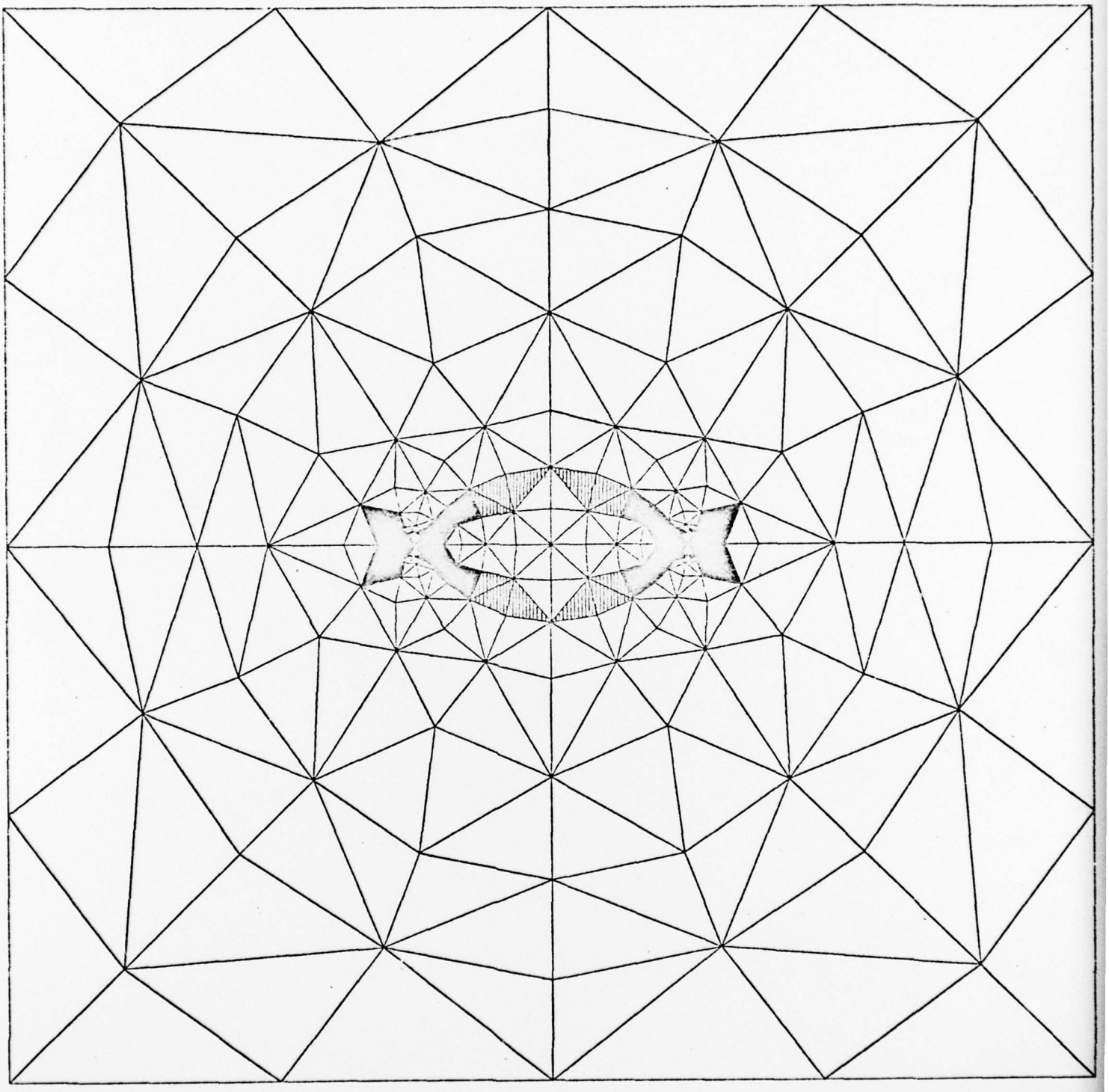

Figure 11e. Cross-hatched area shows octahedral strain exceeding far-field value by 5 percent, and solid area by 10 percent; Poisson constraint, rotation is 90 deg, burst model

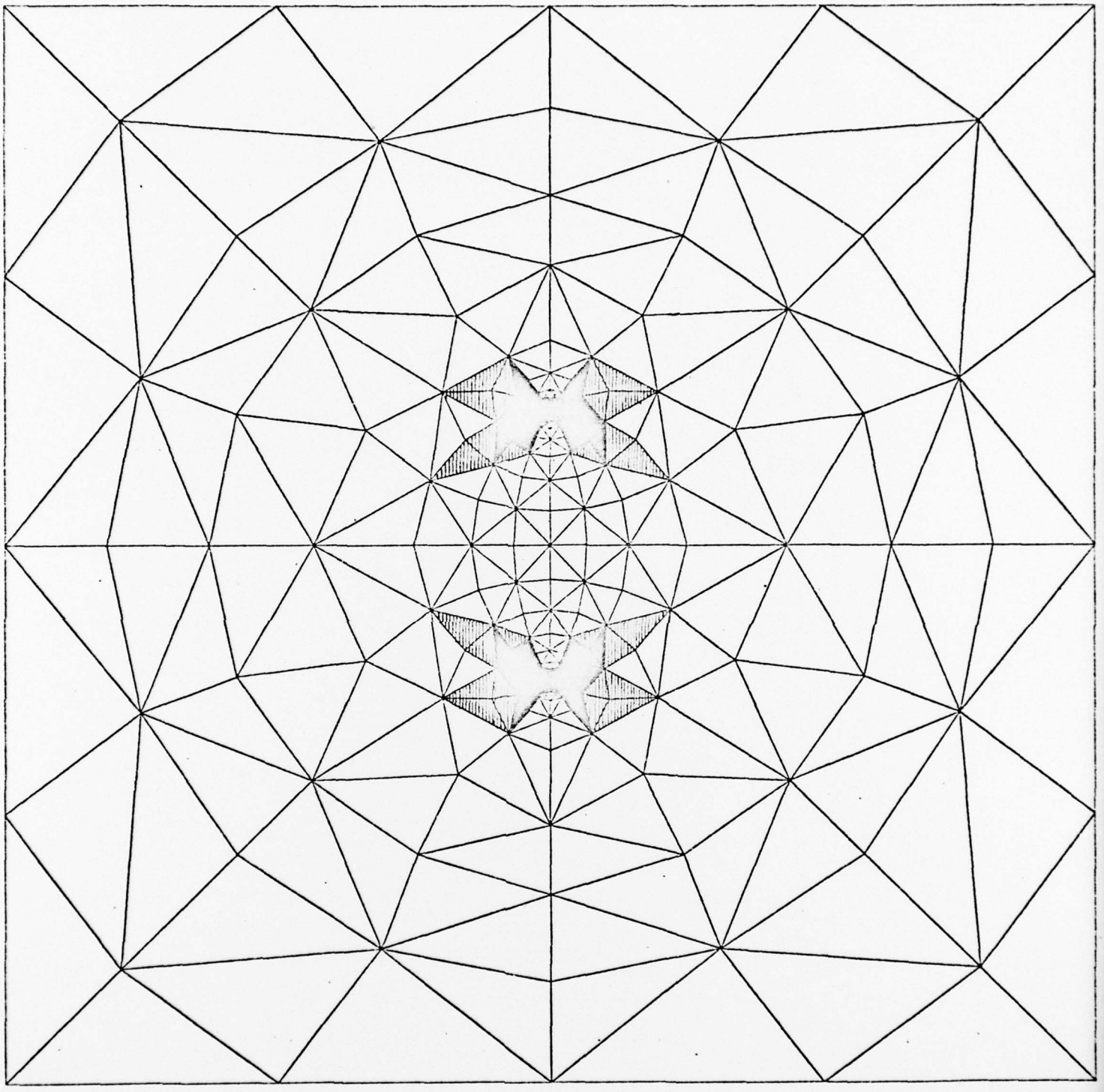

Figure 12a. Cross-hatched area shows octahedral strain exceeding far-field value by 5 percent, and solid area by 10 percent, full constraint, rotation is 0 deg, burst model

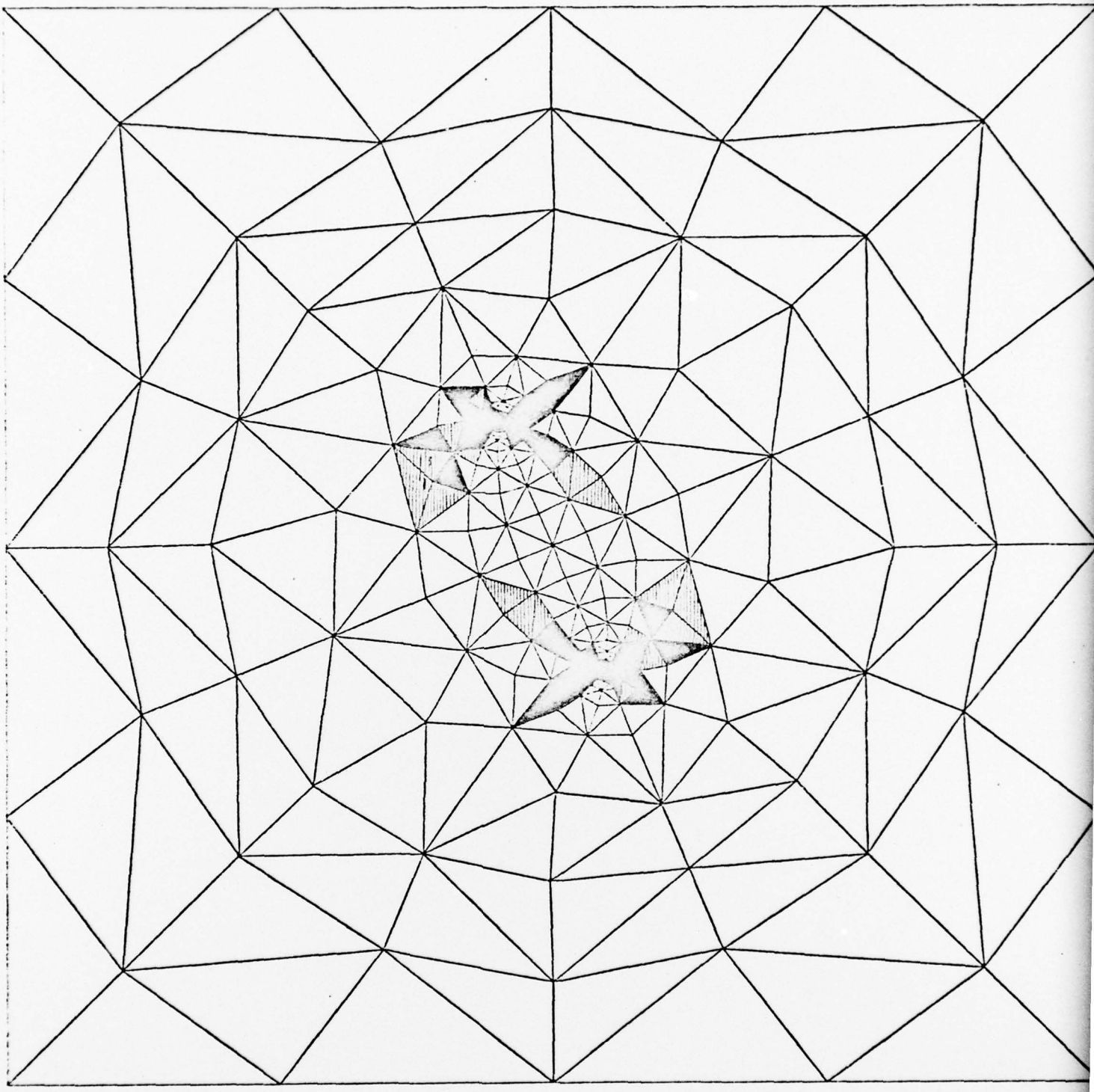

Figure 12b. Cross-hatched area shows octahedral strain exceeding far-field value by 5 percent, and solid area by 10 percent; full constraint, rotation is 22.5 deg, burst model

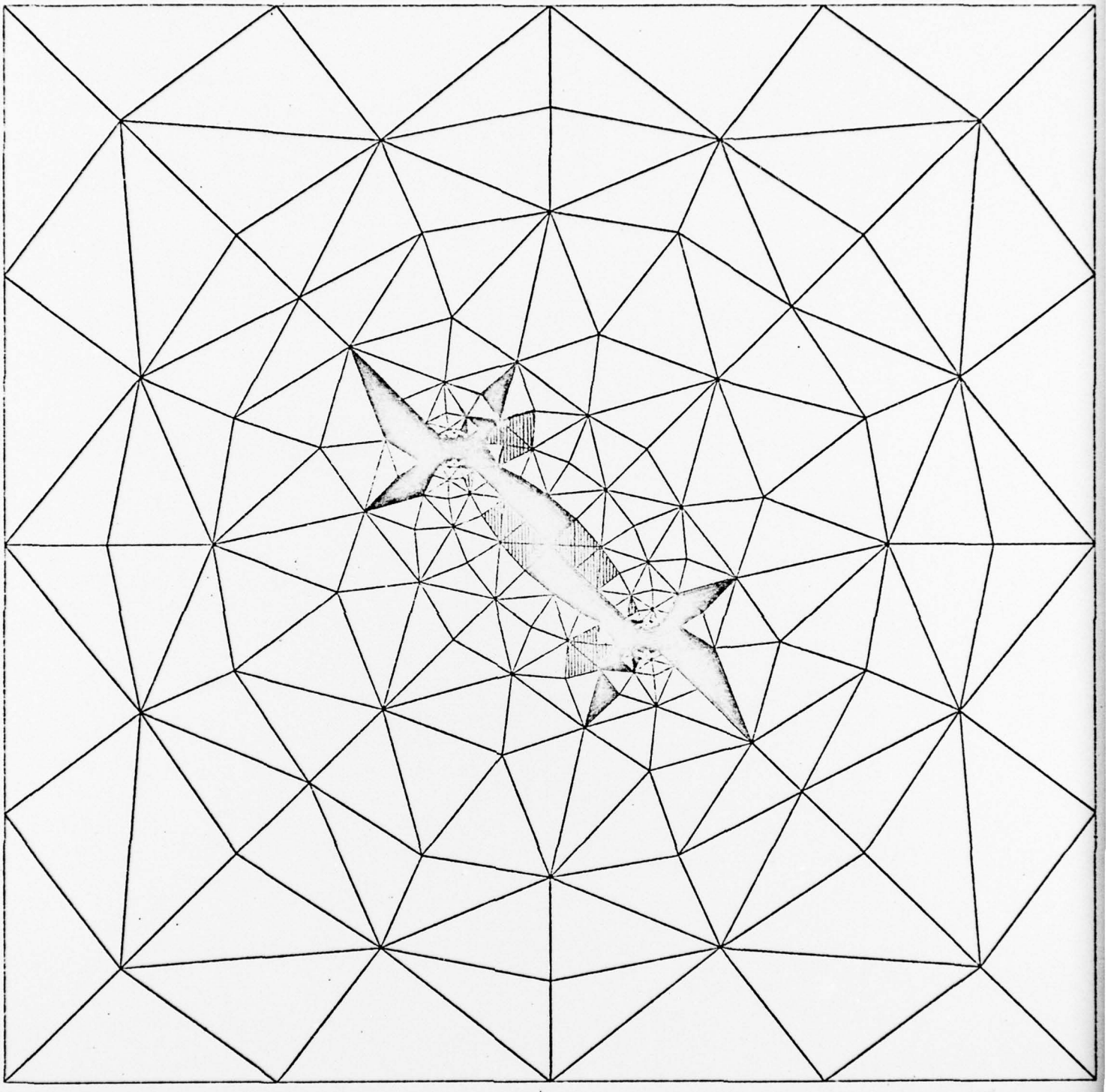

Figure 12c. Cross-hatched area shows octahedral strain exceeding far-field value by 5 percent, and solid area by 10 percent; full constraint, rotation is 45 deg, burst model

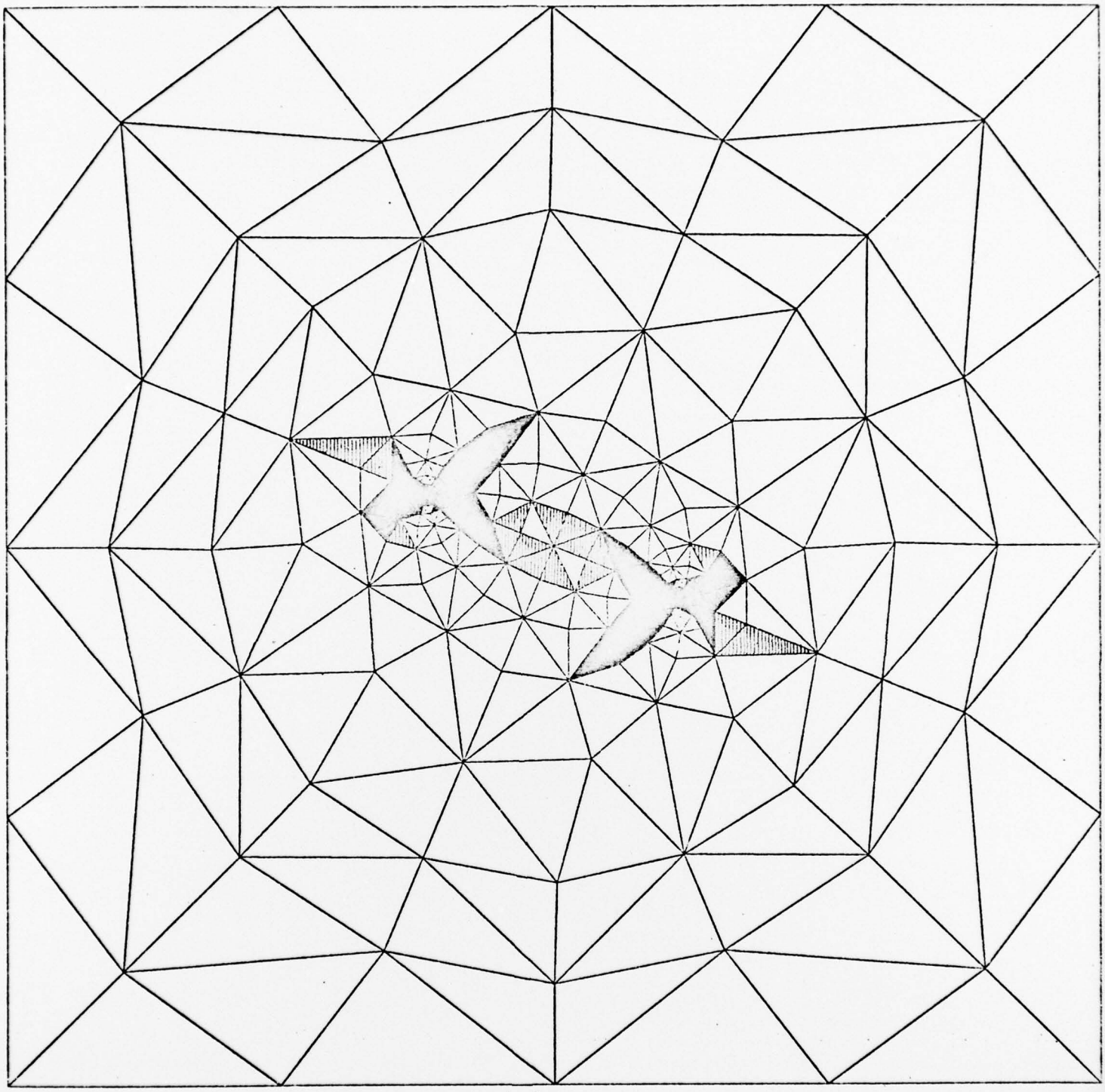

Figure 12d. Cross-hatched area shows octahedral strain exceeding far-field value by 5 percent, and solid area by 10 percent; full constraint, rotation is 67.5 deg, burst model

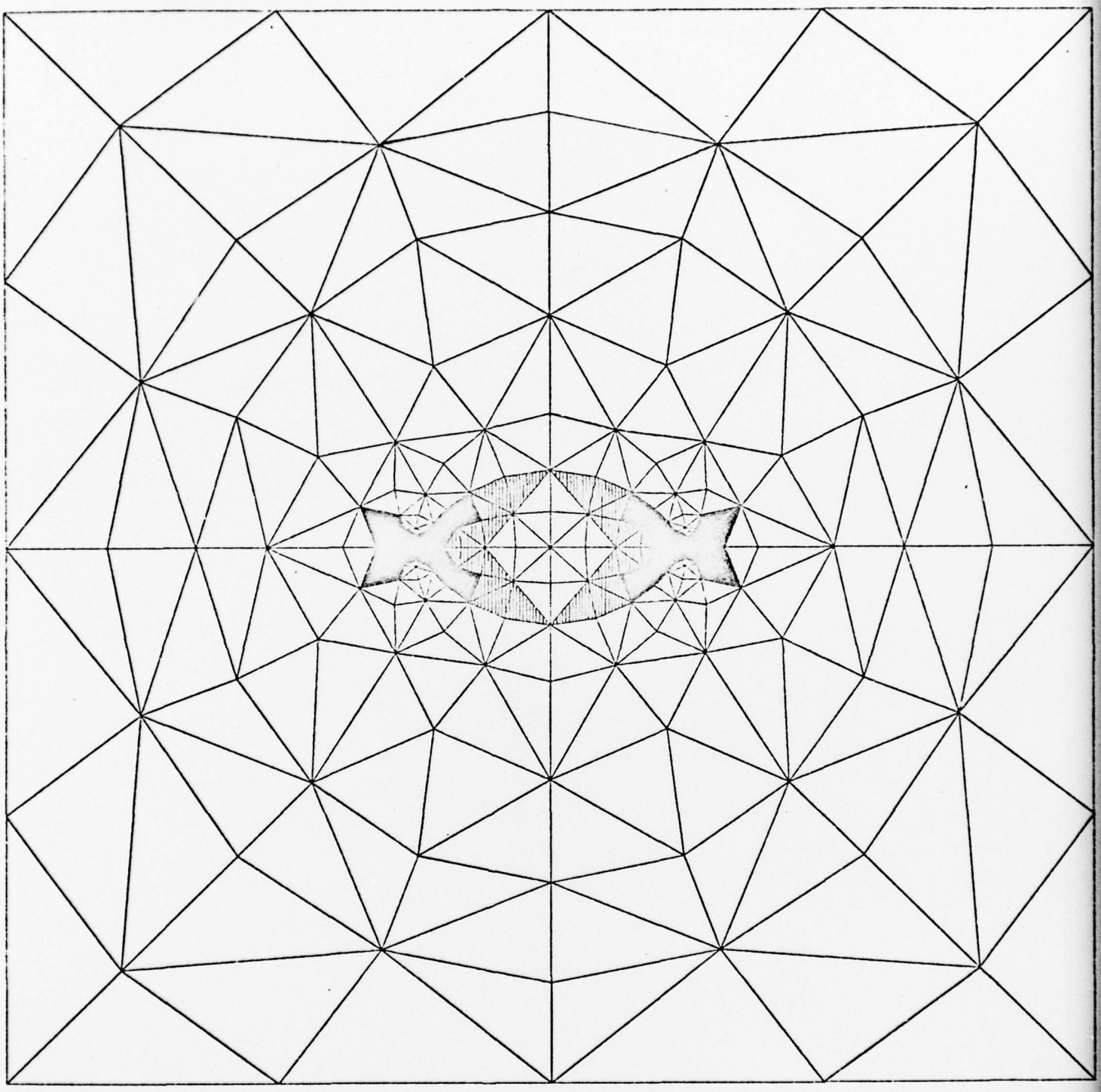

Figure 12e. Cross-hatched area shows octahedral strain exceeding far-field value by 5 percent, and solid area by 10 percent; full constraint, rotation is 90 deg, burst model